

The predictability of near-coastal currents using a baroclinic unstructured grid model

Cheryl Ann Blain · Mustafa Kemal Cambazoglu ·
Robert S. Linzell · Kendra M. Dresback ·
Randall L. Kolar

Received: 1 March 2011 / Accepted: 13 October 2011 / Published online: 28 December 2011
© Springer-Verlag (outside the USA) 2011

Abstract A limited domain, coastal ocean forecast system consisting of an unstructured grid model, a meteorological model, a regional ocean model, and a global tidal database is designed to be globally relocatable. For such a system to be viable, the predictability of coastal currents must be well understood with error sources clearly identified. To this end, the coastal forecast system is applied at the mouth of Chesapeake Bay in response to a Navy exercise. Two-day forecasts are produced for a 10-day period from 4 to 14 June 2010 and compared to real-time observations. Interplay between the temporal frequency of the regional model boundary forcing and the application of external tides to the coastal model impacts the tidal characteristics

of the coastal current, even contributing a small phase error. Frequencies of at least 3 h are needed to resolve the tidal signal within the regional model; otherwise, externally applied tides from a database are needed to capture the tidal variability. Spatial resolution of the regional model (3 vs 1 km) does not impact skill of the current prediction. Tidal response of the system indicates excellent representation of the dominant M_2 tide for water level and currents. Diurnal tides, especially K_1 , are amplified unrealistically with the application of coarse 27-km winds. Higher-resolution winds reduce current forecast error with the exception of wind originating from the SSW, SSE, and E. These winds run shore parallel and are subject to strong interaction with the shoreline that is poorly represented even by the 3-km wind fields. The vertical distribution of currents is also well predicted by the coastal model. Spatial and temporal resolution of the wind forcing including areas close to the shoreline is the most critical component for accurate current forecasts. Additionally, it is demonstrated that wind resolution plays a large role in establishing realistic thermal and density structures in upwelling prone regions.

Responsible Editor: Pierre Lermusiaux

This article is part of the Topical Collection on *Maritime Rapid Environmental Assessment*

C. A. Blain (✉)
Oceanography Division, Naval Research Laboratory,
Stennis Space Center, MS 39529, USA
e-mail: cheryl.ann.blain@nrlssc.navy.mil

M. K. Cambazoglu
Department of Marine Science, University of Southern
Mississippi, Stennis Space Center, MS 39529, USA

R. S. Linzell
Technology Solutions Group, QinetiQ North America,
Stennis Space Center, MS 39529, USA

K. M. Dresback · R. L. Kolar
School of Civil Engineering and Environmental Science,
University of Oklahoma, Norman,
OK 73019, USA

Keywords Coastal currents · Predictability ·
Operational forecast system · Wind resolution ·
Coupled models · Unstructured grid models

1 Introduction

The coastal forecast systems sought by Navy planners are ones that retain their robustness regardless of the region of application, are targeted to local areas of interest, and are ones whose products are able to

address the full suite of Navy parameters that impact coastal operations including acoustic communication, mine hunting, and underwater vehicle operations, to name a few (Blain and Preller 2007). For these type of forecast systems, a better understanding of systematic errors is sought in order to optimize construction of the coastal forecast system to minimize error and maximize robustness.

Assessments of the fidelity of a coastal forecast system typically involve comparisons between forecast products and concurrent in situ observations. A bulk error measure for each physical parameter such as water level, temperature, or currents is computed and reported. This error strictly indicates the deviation of a forecast parameter from the observed value at a specific location and window of time, e.g., Allard et al. (2008), Chu et al. (2011), Ko et al. (2008). What it does not indicate are the sources of error that lead to the mismatch between modeled and observed parameters. As coastal forecast systems advance to consider the implementation of sophisticated forms of data assimilation, e.g., Kurapov et al. (2002), Li et al. (2008), quantification of the error sources is increasingly important. An understanding of the error source can not only lead to more effective data assimilation strategies but also better configuration of the coastal forecast system itself, which will ultimately result in improved forecast products.

The aim of this manuscript is to lay the foundation for analyzing forecast products in such a way as to determine the source of the forecast error, not merely quantify the data fit at a particular point in space and time. Both spatial and temporal resolution of the forcing will be examined for its impact on the forecast products. Forms of the forcing include density initialization and boundary specification derived from a regional model, tides, and surface winds. Section 2 first describes a forecast system designed for limited domain, localized forecasts, and relocatable, global application. Section 3 then defines application of the coastal forecast system to waters in the vicinity of Norfolk, VA. The impact of spatial resolution and temporal frequency of the regional model forcing on baroclinic coastal currents is addressed in Section 4. An examination of the predictability of the tidal response follows in Section 5 while Section 6 provides a detailed analysis of the effects of surface wind spatial and temporal resolution on baroclinic coastal current predictions. Conclusions summarize the findings of the paper that both the regional model solution and its forcing frequency as well as the applied wind and its resolution have significant influences on the accuracy of baroclinic coastal current predictions.

2 Description of the coastal forecast system

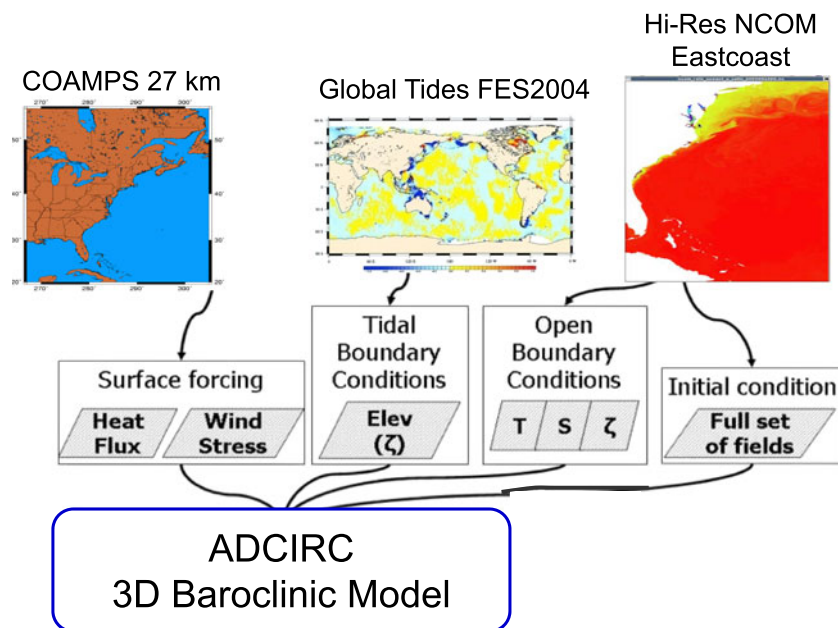
While the core of a coastal ocean forecast system is its coastal ocean model, success is also dependent on access to appropriate real-time surface, initial, and boundary forcing data in the region of interest. This particular coastal forecast system is subject to an additional constraint of portability, meaning that the coastal forecast system must be globally applicable. This restriction serves to narrow the sources from which real-time surface, initial, and boundary forcing data are obtained. A schematic of the forecast system applied herein is depicted in Fig. 1. Components include a core simulator of coastal dynamics (the Advanced Circulation Model, ADCIRC (Luettich and Westerink 2004)), a regional ocean model (the Navy Coastal Ocean Model, NCOM (Barron et al. 2006)) that supplies initial and boundary forcing, a meteorological model (the Coupled Ocean–Atmosphere Mesoscale Prediction System, COAMPS^{TM,1} (Hodur 1997)) from which surface meteorological forcing is derived, and a global tidal database (FES2004 (Lyard et al. 2006)). Detailed descriptions of each component and their inter-relationships with one another are discussed subsequently. Similar variants of this same forecast system using the ADCIRC model as the dynamical core have been applied to the northern Gulf of Mexico (Dresback et al. 2010) and the Turkish Strait System (Blain et al. 2009).

2.1 The coastal circulation model

To capture the coastal circulation dynamics in near-coastal waters at high resolution, the baroclinic form of the coastal circulation model ADCIRC is selected as the dynamical engine of the coastal forecast system. The finite element basis of the ADCIRC model allows tremendous flexibility in the construction of a computational grid that represents complex shorelines and provides high resolution where desired. ADCIRC is a fully nonlinear, shallow water equation model whose dynamics have recently expanded to include three-dimensional transport and mixing associated with density-driven circulation (Dresback et al. 2010; Kolar et al. 2009). Similar to a number of prominent 3D near-coastal circulation models, e.g., Princeton Ocean Model (Blumberg and Mellor 1987), Estuarine and Coastal Ocean Model (Blumberg et al. 1993), Regional

¹COAMPS is a registered trademark of the Naval Research Laboratory.

Fig. 1 A depiction of the coastal forecast system based on the baroclinic ADCIRC model and its required data flow from one-way coupling to the COAMPS and NCOM models



Ocean Modeling System (Shchepetkin and McWilliams 2005), and Finite Volume Coastal Ocean Model (Chen et al. 2003a), ADCIRC uses a mode-splitting technique to solve the conservation equations. The free surface elevation, obtained from an external mode solution of the depth-averaged continuity equation, forces the internal mode solution, which resolves the horizontal velocity field using a stretched sigma-coordinate system (Dresback 2005; Luettich and Westerink 2004). The 3D continuity equation is solved for the vertical velocity, subject to kinematic boundary conditions (Luettich et al. 2002; Muccino et al. 1997). For the baroclinic simulations, ADCIRC solves the time-dependent scalar transport equation for salinity and temperature. Through the equation of state described by McDougall et al. (2003), ADCIRC uses the temperature, salinity, and pressure in determining the density field. In order to avoid spurious currents for stably stratified flow, the baroclinic pressure gradients are evaluated in a level coordinate system and are fed back into the momentum equation through the buoyancy term (Dresback 2005; Dresback et al. 2004). Recent validation efforts by Kolar et al. (2009) report accurate propagation of the shape and position of a density front in the classic density-driven lock-exchange problem. Furthermore, Blain et al. (2009) demonstrate the capability of ADCIRC to capture two-layer estuarine flow in the Dardanelles Strait at high resolution, in an application of ADCIRC to the complex Turkish Strait System.

The standard configuration of the ADCIRC model for coastal forecasting includes selection of the Mellor–Yamada 2.5 level closure (Burchard 2002; Mellor and

Yamada 1982) to represent vertical mixing using a specified minimum vertical eddy viscosity coefficient equal to $0.00001 \text{ m}^2 \text{ s}^{-1}$. The model applies a linear slip at the ocean bottom with a linear friction coefficient of 0.005. Spatially constant values of 0.01 (m) and 0.0001 (m) are used for free surface and bottom roughness, respectively, and a spatially constant horizontal eddy viscosity value of $50 \text{ m}^2 \text{ s}^{-1}$ is specified within the momentum equations, based on the work of Westerink et al. (2008). The weighting parameter, τ_0 , in the generalized wave continuity equation is spatially variable with values of 0.005 in water depths greater than 200 m. For water depths between 1 and 200 m, τ_0 is specified as $1/\text{depth}$ and for depths less than 1 m, τ_0 is set to a value of 1.0. This variability of the τ_0 parameter results in better stability and mass conservation properties of the model solution. Wetting and drying is inactive in the present implementation of the baroclinic coastal forecast system.

2.2 Meteorological forcing

The need for global coverage, real-time availability, and mesoscale atmospheric dynamics leads to selection of the Naval Research Laboratory’s COAMPS (Chen et al. 2003b) to provide the surface meteorological forcing. The atmospheric portion of COAMPS represents a complete three-dimensional data assimilation system comprised of data quality control, analysis, initialization, and forecast model components. The types of mesoscale phenomena to which COAMPS has been applied include mountain waves, land–sea

breezes, terrain-induced circulations, tropical cyclones, mesoscale convective systems, coastal rainbands, and frontal systems. The atmospheric model within COAMPS uses nested grids to achieve high resolution for a given area; it contains parameterizations for sub-grid scale mixing, cumulus formulation, radiation, and explicit moist physics (Hodur 1997). Forecast variables used by the baroclinic coastal circulation model include 10-m surface wind velocities, atmospheric pressure, shortwave and longwave radiation, and sensible and latent heat fluxes. The COAMPS surface wind fields are converted to wind stress using the formulation of Garratt (1977). The total surface heat flux is estimated using the relation presented by Mellor (1996) together with forecast data for net shortwave and longwave radiation, and latent and sensible heat fluxes from the COAMPS model.

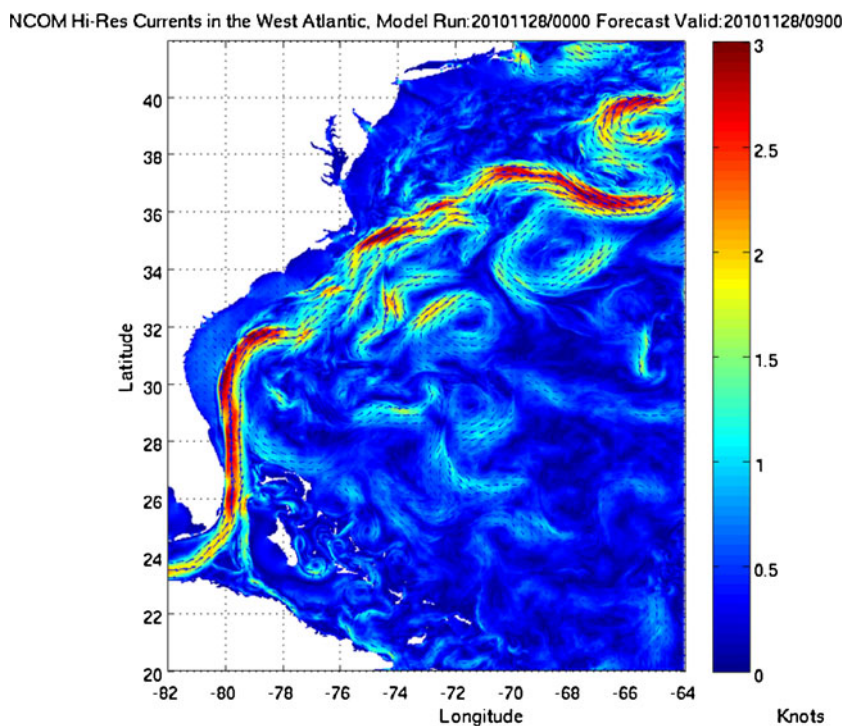
2.3 Initialization and boundary forcing

Temperature, salinity, elevation, and velocity fields from a regional ocean model are needed both to initialize the spin-up phase of the forecast cycle and, in part, provide boundary forcing values to the coastal model along the open water boundary throughout the duration of the forecast. Considering the need for global applicability of the developed baroclinic coastal forecast system, the NCOM is selected to be the source

for regional ocean conditions; the NCOM, GOFS v2.6, runs operationally at the Naval Oceanographic Office (Barron et al. 2004; Kara et al. 2006) and has global coverage should high-resolution (Hi-Res) regional NCOM implementations be unavailable. The selection of a single model (i.e., NCOM) from which initial and boundary forcings are derived simplifies development of the interface between the coastal and regional model.

For the study described herein, regional model fields are obtained from the National Centers for Environmental Prediction (NCEP) which publishes the operational NCOM fields for US coastal waters (NCEP 2010). A Hi-Res implementation of NCOM is applied to the US east coast over the domain shown in Fig. 2 at a resolution of $1/36^\circ$ (or approximately 3 km). The surface wind, heat, and salt fluxes applied to NCOM originate from the 0.5° Navy Global Atmospheric Prediction System (NOGAPS) (Rosmond et al. 2002). To improve detail of the upper-ocean dynamics, NCOM maintains a maximum 1-m upper level thickness in a hybrid sigma/ z vertical configuration (Barron et al. 2006) with 35 terrain-following sigma levels in the upper 641 m over 15 fixed-thickness z -levels extending to a maximum depth of 5,500 m. Model depth and coastline are based on a global 2-min bathymetry produced at the Naval Research Laboratory. Tidal variations are included by superimposing tidal values extracted from the OSU TPXO6 database (Egbert and Erofeeva

Fig. 2 Surface currents on 28 November 2010 from the 3-km NCOM Hi-Res Eastcoast regional model



2002; Egbert et al. 1994) onto the prescribed initial and boundary conditions.

Initial conditions for the baroclinic coastal forecast system are determined by the density field that is derived from a diagnostic run of the baroclinic ADCIRC model, initialized by NCOM regional model temperature and salinity values. During the diagnostic simulation, the density field taken from NCOM is held constant while applied tides and winds are ramped from zero to their full value over 3 days. The resulting diagnostic solution for temperature, salinity, velocity, and elevation defines the initial conditions for a baroclinic ADCIRC forecast run. The NCOM and ADCIRC temperature and salinity fields used for initialization are evaluated in Section 4. Following the diagnostic calculations, a 3-day prognostic forecast period follows during which winds, surface heat flux, tides, and the density structure, as computed by the baroclinic ADCIRC model, all evolve in time.

Boundary forcing at the open ocean limit of the ADCIRC baroclinic coastal model is specified by assigning water elevations as well as temperature and salinity over the water column from the regional NCOM solution at open boundary points on a daily frequency. A 12-km temporally invariant, spatial ramp, or sponge layer for application to wind and advection terms within ADCIRC computations is utilized in this application. The interpolation or extrapolation of the regional model solution to ADCIRC model grid nodes for either initialization or boundary forcing follows a distance weighted interpolation scheme as described in Dresback et al. (2010). Tidal variability entering the coastal model domain is captured by applying tides from a global database. Nine tidal constituents (M_2 , S_2 , N_2 , K_2 , K_1 , O_1 , Q_1 , P_1 , and $2N_2$) are extracted from the global tidal database, FES2004 (Lyard et al. 2006), and prescribed as known elevations along the open ocean boundary. The tidal potential body forcing is inactive for both the regional model and the coastal model, ADCIRC. Recall that the tidal signal is also present in the NCOM regional model solutions; this apparent redundancy is addressed in the analysis and discussion herein.

3 Application at the mouth of Chesapeake Bay, VA

The desire for baroclinic coastal ocean forecasts in the local area indicated by the bounding box in Fig. 3 provides an opportunity to evaluate the performance of the limited domain, baroclinic coastal forecast system just described. Forecasts target waters surrounding the US Naval Station at Norfolk, VA located just over

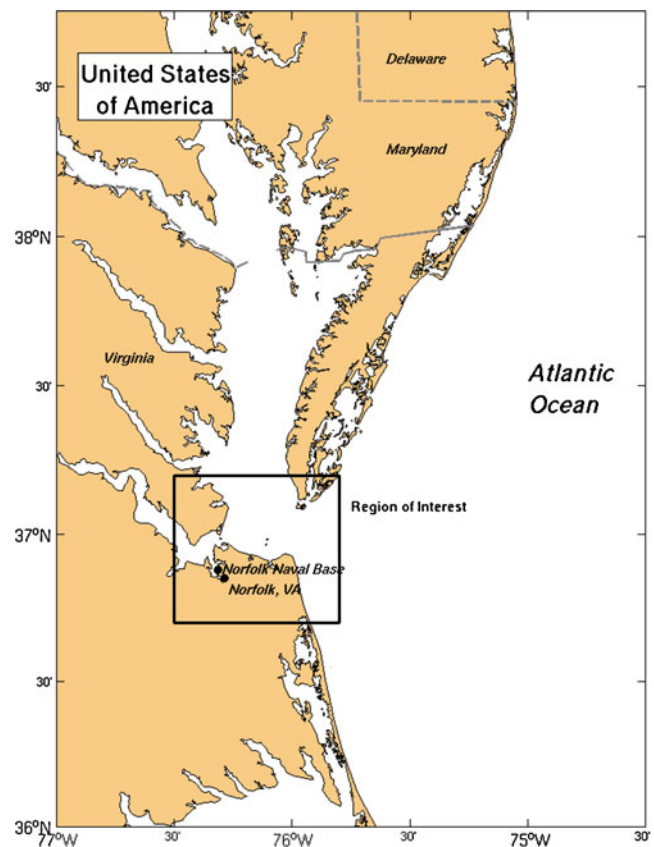
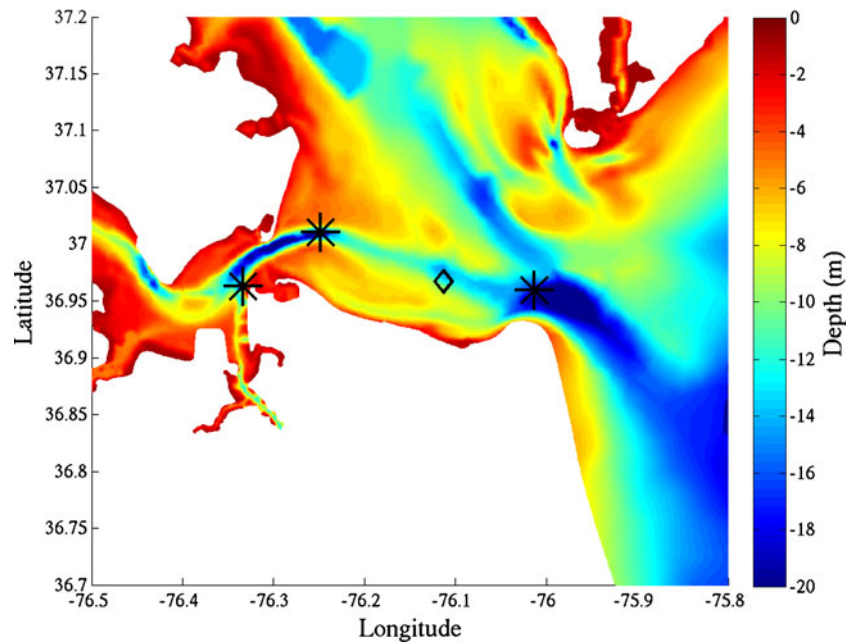


Fig. 3 Region of interest (contained within the bounding box) near the US Naval Station, Norfolk, VA, located in the southwestern corner of Chesapeake Bay near its mouth

33 km west of the entrance to the Chesapeake Bay from the Atlantic Ocean. The dominant bathymetric feature in the area is the Thimble Shoal Channel; the National Oceanic and Atmospheric Administration (NOAA) station at Thimble Shoal and the seaward extension of that channel are evident in the bathymetry contours shown in Fig. 4. The shipping channels by law are maintained at a minimum depth of 45 ft (13.7 m). Outside the shipping channels and with the exception of areas close to shore, the NOAA developed bathymetry (Yang et al. 2007) indicates average water depths of just less than 6 m. Li et al. (2005) describe the surrounding estuarine flow as composed of a freshwater plume at the surface that moves seaward from Chesapeake Bay entrance, tending to the western shore, and highly saline ocean water that flows landward through deeper channels, such as Thimble Shoal. Moderate tidal fluctuations and episodic winds of periods 2–7 days modulate the stratified flow. The James River, entering from the west, on average, contributes less than 7,000 cfs of freshwater into the area, with even lower flow conditions during the summer months.

Fig. 4 Depth in meters and locations of the NOAA ADP stations (*stars*, west to east), Naval Station Norfolk, Thimble Shoal, and Cape Henry, and the NOAA water level station (*diamond*) at Chesapeake Bay Bridge Tunnel



Available current observations include three NOAA real-time acoustic Doppler profilers (ADPs) archiving at 6-min intervals in 1-m vertical bins identified by stars in Fig. 4 from inshore to offshore, Naval Station Norfolk (NOAA Station ID: CB0402), Thimble Shoal (NOAA Station ID: CB0301), and Cape Henry (NOAA Station ID: CB0102), respectively. A water level station at Chesapeake Bay Bridge Tunnel (NOAA Station ID: CBBV2-8638863), located between Thimble Shoal and Cape Henry (shown as a diamond in Fig. 4), also records real-time data.

To minimize the effects of prescribed boundary values on the local waters of interest, a computational

domain, shown in Fig. 5, is constructed to have an offshore boundary that begins near Bay Head, NJ; extends eastward beyond the shelf into waters greater than 2,000 m depth; and intersects land to the south at Nags Head, NC. This finite element mesh is composed of 192,051 triangular elements containing 99,309 triangle vertices or computational nodes. Spatial resolution, as evident by the increasing density of the elements as water becomes shallower in Fig. 5, ranges from 14 km offshore to 120 m in the shallowest, near-coastal waters. The resolution refinement of the mesh generally follows a topographic length scale ($\Delta H/H$, where H is the average element depth and ΔH is the change in

Fig. 5 The finite element mesh applied to forecasts in the vicinity of Norfolk, VA

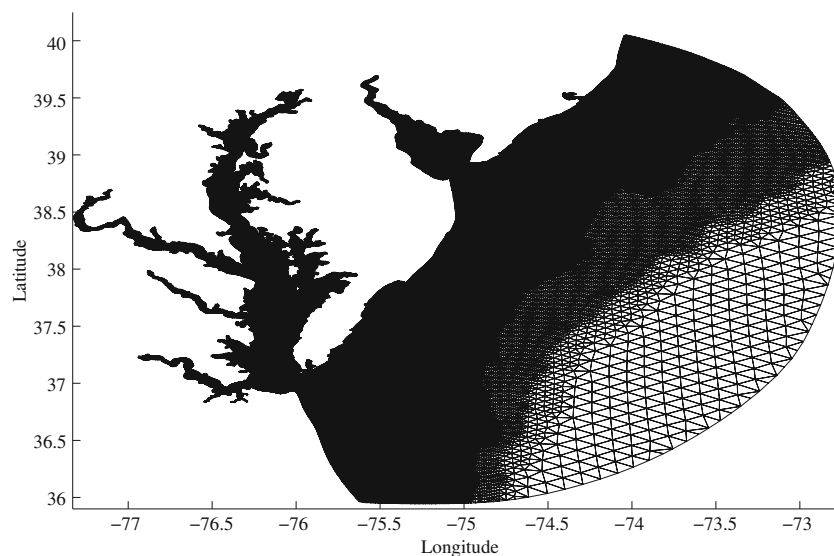
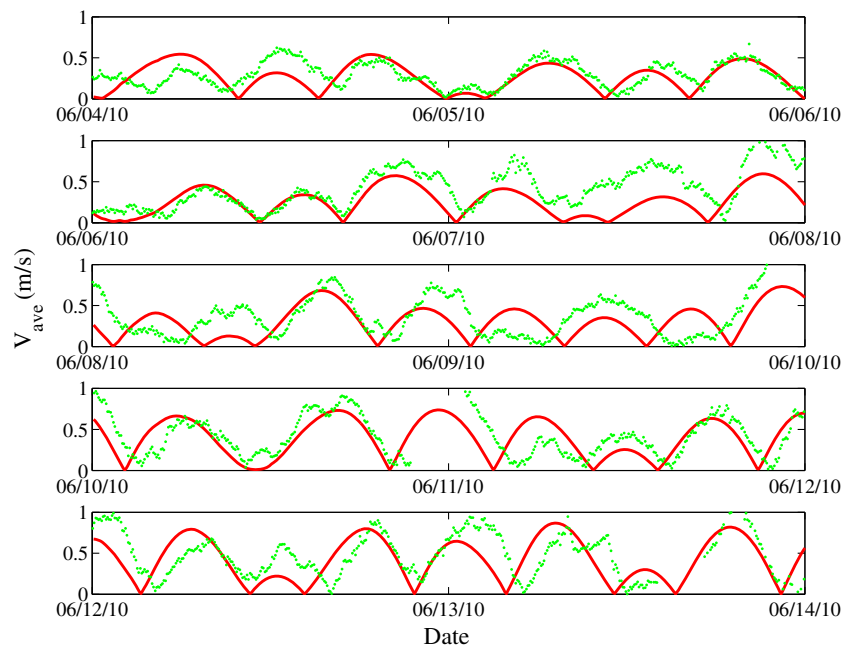


Fig. 6 Two-day model forecasts of baroclinic (depth-averaged) currents (red) compared to observed (depth-averaged) currents (green) from 4 to 14 June



depth within an element) (Hannah and Wright 1995) between 0.1 and 0.6. The water column is discretized using 41 uniformly distributed sigma levels.

For the period of 4–14 June 2010, the ADCIRC baroclinic coastal forecast system is applied to the domain described and executed daily to produce 72-h forecasts of water level, 3D currents, temperature, and salinity. The 6-day diagnostic–prognostic forecast cycle consumes 4 h of CPU time on 64 2.8 GHz processors. High spatial (150 m resolution) and dense temporal (i.e., hourly; 6 min at stations) resolution forecast products are generated for the area that extends from the mouth of the James River, VA to waters east of Cape Henry, VA and includes the Naval Station piers at Norfolk (a region identical to that shown in Fig. 4).

Forecasts of the 3D baroclinic currents (displayed as depth-averaged values) are compared to observed currents (also depth-averaged for display) in Fig. 6 in 2-day increments for the entire 10-day period in June 2010. During the first 2-day period, 4–6 June, current

magnitudes agree well with observations on two flood cycles but vacillate between over- and underprediction for the remaining flood stages. A similar inconsistency in current magnitude predictions is observed from 12 to 14 June. The remaining forecast periods have marked underprediction of the current magnitude. A 1- to 2-h phase error is evident and persists during all forecast periods with the exception of 6–8 June when the phase error is less pronounced. Quantitative comparisons between modeled and observed baroclinic currents for the same 2-day forecast periods are given in Table 1 at Cape Henry. The root mean square error (RMSE) and the correlation coefficient (R^2) are reported to provide separate skill indicators for magnitude and phase of the currents, respectively. The Wilmott (1981) skill score is also included as a bulk measure of skill and to facilitate comparison to other modeling efforts at this location, e.g., Blumberg and Goodrich (1990), Li et al. (2005). The low RMSE (0.171) during the first forecast period (4–6 June) reflects some coincidence of

Table 1 Baroclinic current (depth-averaged) error statistics at Cape Henry for 27-km winds

Date	RMSE (m/s)	R^2	Wilmott skill score
4–6 June	0.171	0.381	0.618
6–8 June	0.256	0.545	0.624
8–10 June	0.280	0.469	0.606
10–12 June	0.206	0.649	0.787
12–14 June	0.281	0.496	0.688

RMSE root mean square error, R^2 correlation coefficient

Table 2 Baroclinic current (depth-averaged) error statistics at Thimble Shoal for 27-km winds

Date	RMSE (m/s)	R^2	Wilmott skill score
4–6 June	0.151	0.237	0.545
6–8 June	0.141	0.429	0.826
8–10 June	0.183	0.223	0.679
10–12 June	0.187	0.211	0.664
12–14 June	0.187	0.563	0.772

RMSE root mean square error, R^2 correlation coefficient

Table 3 Baroclinic current (depth-averaged) error statistics at Naval Station Norfolk for 27-km winds

Date	RMSE (m/s)	R^2	Wilmott skill score
4–6 June	0.215	−0.270	0.361
6–8 June	0.201	0.021	0.689
8–10 June	0.194	0.084	0.595
10–12 June	0.226	0.337	0.611
12–14 June	0.253	0.192	0.612

RMSE root mean square error, R^2 correlation coefficient

the current magnitude with observations, but the low correlation coefficient (0.381) is indicative of significant phase errors. For the period 6–14 June, the error statistics are fairly consistent across the 2-day forecast periods, averaging 25 cm/s of RMSE and R^2 ranging from 47% to 65%. While the magnitude of the current error exceeds what would be considered acceptable, the inconsistency of the forecast accuracy through time is particularly troubling and suggests that there may be larger errors associated with certain coastal processes. Errors at the two other stations, Thimble Shoal and Naval Station Norfolk, are reported in Tables 2 and 3, respectively. The RMSE errors are typically larger while correlations and Wilmott scores trend lower as one moves further inshore. The decreasing fidelity indicates that the forecast system, at times, is not capturing smaller-scale dynamics that would dominate circulation at these near-coastal stations. The remainder of this paper focuses on uncovering the sources of current prediction error in the configured baroclinic coastal forecast system.

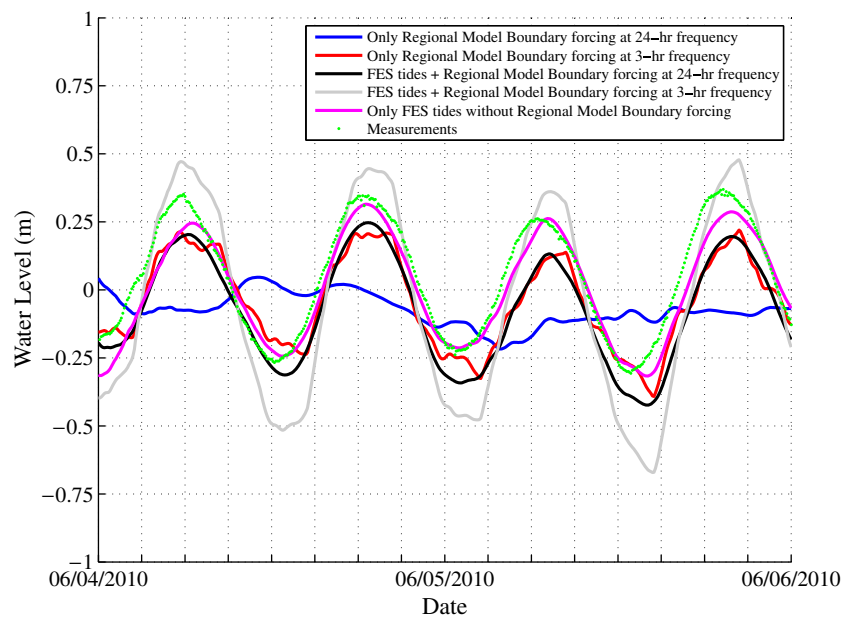
4 Impact of the regional model

The application of boundary forcing derived from the regional model can be a significant source of error in representing tidal variability (Logutov and Lermusiaux 2008) as well as the underlying density structure. For the baroclinic coastal model, ADCIRC, initial and boundary forcing fields are supplied by the Hi-Res NCOM regional model as described in Section 2.3. Recall that the spatial resolution of the Hi-Res NCOM fields is 3 km and temporal frequency of the products is daily (24 h). The effects of the tides are included within the regional model solution (see Section 2.3). Additionally, within the operational configuration, tidal elevation forcing (extracted from FES2004) is superimposed on regional model elevations applied at the open ocean boundary. Initially, the accuracy of tides extracted from the FES2004 database is verified at the open boundary

through comparison to tides extracted from the tidal database, EC2001 (Mukai et al. 2002), which has been extensively validated for the northwestern coast of the Atlantic basin. Correlation coefficients of greater than 99% and root mean square errors of 2.87 cm confirm that the FES2004 database itself is not a significant source of error.

To better understand how the tidal variability imposed at the open ocean boundary influences the nearshore water level and current predictions, the computed and observed water levels at the Chesapeake Bay Bridge Tunnel Station for the period 4–6 June 2010 are analyzed. Displayed in Fig. 7 are the effects of an increasing temporal frequency of the regional model (24 vs 3 h) as well as the inclusion or exclusion of the externally applied tidal forcing from the FES2004 database along with measured water levels (green). Water levels from the daily (24-h) regional model solution (blue) deviate from mean sea level by less than 20 cm and exhibit a very long wave, residual tidal response. Increasing the regional model frequency to 3 h (red) results in a stronger semi-diurnal tidal oscillation that overpredicts (underpredicts) the ebb (flood) tide and lags in phase from 90 min to 2 h as compared to the observations. While the tidal signal is better resolved with the higher-frequency boundary forcing, notable discrepancies in the water level remain. The water level response is similar when tides from the FES2004 database are superimposed on the daily (24-h) regional model solution (black), albeit a less noisy solution having a slight reduction in phase error on flood. If tidal forcing is derived from both an external application of tides and tidal oscillations are evident in regional model forcing applied at high frequency (3 h) (gray), the tidal variations are over-amplified as these effects are additive. To separate the influence of the regional model, the computed water levels subject only to externally applied tides (magenta) are considered. These water levels actually compare most favorably to the observations. Magnitudes on flood and ebb are notably improved, and though a phase lag remains, it is less than 1 h. The inclusion of low-frequency regional model elevations (black) disrupts the natural tidal signal (magenta) and negatively impacts the prediction of water level. Statistical errors for the water levels presented in Fig. 7 when compared to the measured data are found in Table 4. The values in columns 4 (5) in Table 4 are the statistical errors associated with the red (black) line in Fig. 7. The quantitative error measures support the conclusions above that higher-frequency (i.e., three-hourly) boundary forcing from the regional model is necessary to capture any significant tidal oscillation and that external tide application directly to

Fig. 7 The influence of boundary forcing on predicted water levels using regional model forcing frequencies of 24 h (blue) and 3 h (red) without external tides, regional model forcing frequencies of 24 h (black) and 3 h (gray) with external tides applied, and the external tides alone (magenta). Measured water levels (green) at Chesapeake Bay Bridge Tunnel are also shown



the coastal model better captures the fundamental tidal variability present. The lowest RMSE and the highest correlation coefficients (column 7, magenta) actually occur when tides are applied externally to the coastal model and no water levels from the regional model are introduced. The external tidal forcing is applied at the open boundary in the form of constituent data, and the time variability is computed on a per timestep basis (on the order of seconds), indicating that non-linear tidal constituents that have shorter wavelengths (and thus need greater temporal frequency to resolve them) may be important in these shallow coastal waters. As will be discussed subsequently, the over-/underprediction of the water level is correlated to accuracy of the predicted currents.

Predicted currents subject to the same regional model forcing frequencies and application of the external tide are shown in Fig. 8. The corresponding statistics computed for the forecast currents are recorded in

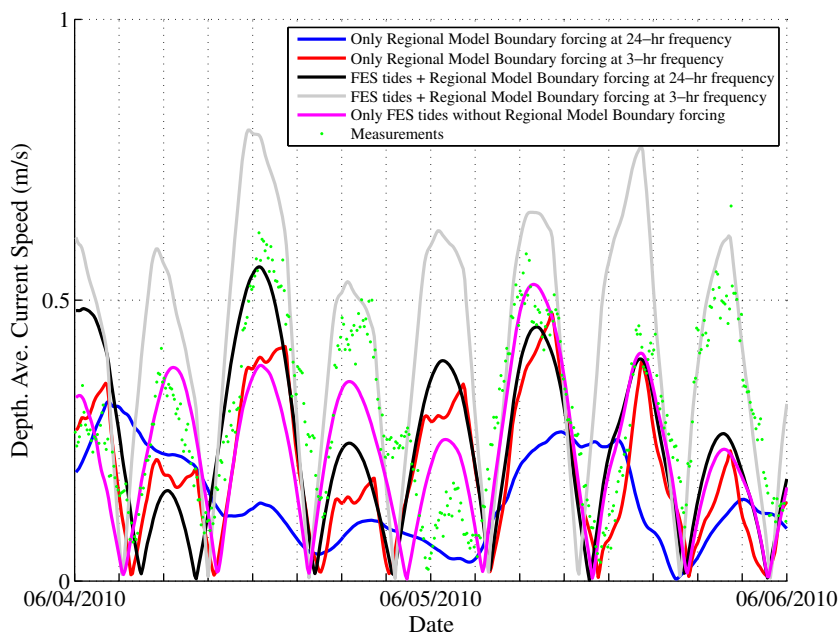
Table 5. For currents, the lack of tidal signal in the daily regional model fields is evident (blue line in Fig. 8). Once either the frequency of the regional model forcing is increased to 3 h (red) or the tides are applied externally to the coastal model (black), the predicted currents are similar. Those currents derived using high-frequency regional model forcing and no external application of tides tend to be noisier at peak magnitudes. On flood tide (even peaks in Fig. 8, if peak 1 is at 0 h on 4 June 2010), recall water levels are best predicted when only the external tides from FES2004 are included as boundary forcing (magenta in Fig. 7). Correspondingly, the flood currents reflect the observed currents best when using this same open ocean boundary elevation forcing. Exceptions are for flood tides at peaks 4 and 8, where the addition of the high-frequency regional model solution leads to an improved current prediction (gray). This suggests that perhaps important interactions occur between high-frequency tides and that

Table 4 Water level error statistics at Chesapeake Bay Bridge Tunnel/varied regional model forcing frequency and tide forcing configuration

Date		Only NCOM		NCOM + FES		Only FES
		24 h	3 h	24 h	3 h	
4–6 June	RMSE	0.2126	0.0758	0.0462	0.1542	0.0513
	R^2	-0.0110	0.9387	0.9749	0.9729	0.9694
6–8 June	RMSE	0.2267	0.1017	0.0937	0.2019	0.0883
	R^2	-0.0795	0.8778	0.9001	0.9117	0.9112
8–10 June	RMSE	0.2494	0.0878	0.0727	0.2264	0.0585
	R^2	-0.1902	0.9305	0.9551	0.9597	0.9700
10–12 June	RMSE	0.2765	0.0934	0.1053	0.2854	0.0848
	R^2	0.3013	0.9467	0.9457	0.9579	0.9613
12–14 June	RMSE	0.3209	0.0988	0.0806	0.3038	0.0748
	R^2	0.1102	0.9531	0.9722	0.9677	0.9756

RMSE root mean square error, R^2 correlation coefficient

Fig. 8 The influence of boundary forcing on predicted baroclinic currents (depth-averaged) using regional model forcing frequencies of 24 h (blue) and 3 h (red) without external tides, regional model forcing frequencies of 24 h (black) and 3 h (gray) with external tides applied, and the external tides alone (magenta). Measured currents (depth-averaged) (green) at Cape Henry are also shown



other processes computed within the regional model contribute in a non-negligible way to the predicted currents. A spectral analysis of the measured currents (not shown) indicates current magnitudes of 2–3 cm/s at high frequencies of 0.2–0.4 cycles/h, reinforcing the importance of non-linear tidal interactions in these near-coastal waters.

On ebb tide, the influence of the boundary forcing is less direct. Generally, the underprediction of water level results in faster currents (peak 5, black) than observed. Though application of the FES2004 tides alone at the boundary generally results in the best match of computed and observed currents, there are times when the regional model signal is influential (e.g., peak 3). This analysis clearly demonstrates that the applied elevation forcing at the open ocean can be very influential in the prediction of coastal currents, yet errors in that forcing are difficult to diagnose due to the complexity of the non-linear interactions in shallow

water. While correction of the applied boundary values through an assimilation scheme is beyond the scope of this manuscript, the methodology of Logutov (2008) as demonstrated in Dabob Bay/Hood Canal, WA by Logutov and Lermusiaux (2008) could provide a viable means for correcting this source of error in the future.

Another source of potential error arises from the specified initial condition derived from the regional model and interpolated to the limited domain coastal model. The 3-km, regional NCOM model is interpolated or extrapolated to the baroclinic ADCIRC coastal model grid nodes following a distance-weighted interpolation scheme. If all regional model grid points surrounding a coastal model node fall on land, an outward expanding circular search is conducted until a sea point on the regional model grid is encountered and its value applied (Dresback et al. 2010). In the vertical, the sigma-z-grid values of the regional model are interpolated to an intermediate z-grid and then further

Table 5 Baroclinic current (depth-averaged) error statistics at Cape Henry/varied regional model forcing frequency and tide forcing configuration

Date		Only NCOM		NCOM + FES		Only FES
		24 h	3 h	24 h	3 h	
4–6 June	RMSE	0.2226	0.1668	0.1601	0.2251	0.1333
	R ²	0.0168	0.5020	0.4682	0.5088	0.6492
6–8 June	RMSE	0.3753	0.2414	0.2590	0.2423	0.2197
	R ²	0.0446	0.6865	0.4867	0.5398	0.6759
8–10 June	RMSE	0.3412	0.1862	0.1608	0.3216	0.2058
	R ²	0.0879	0.8696	0.8521	0.5567	0.7677
10–12 June	RMSE	0.3172	0.2163	0.2776	0.3570	0.2002
	R ²	0.0750	0.6648	0.3630	0.4063	0.6576
12–14 June	RMSE	0.4344	0.2925	0.2999	0.4257	0.2888
	R ²	−0.9399	0.5103	0.4552	0.3600	0.4560

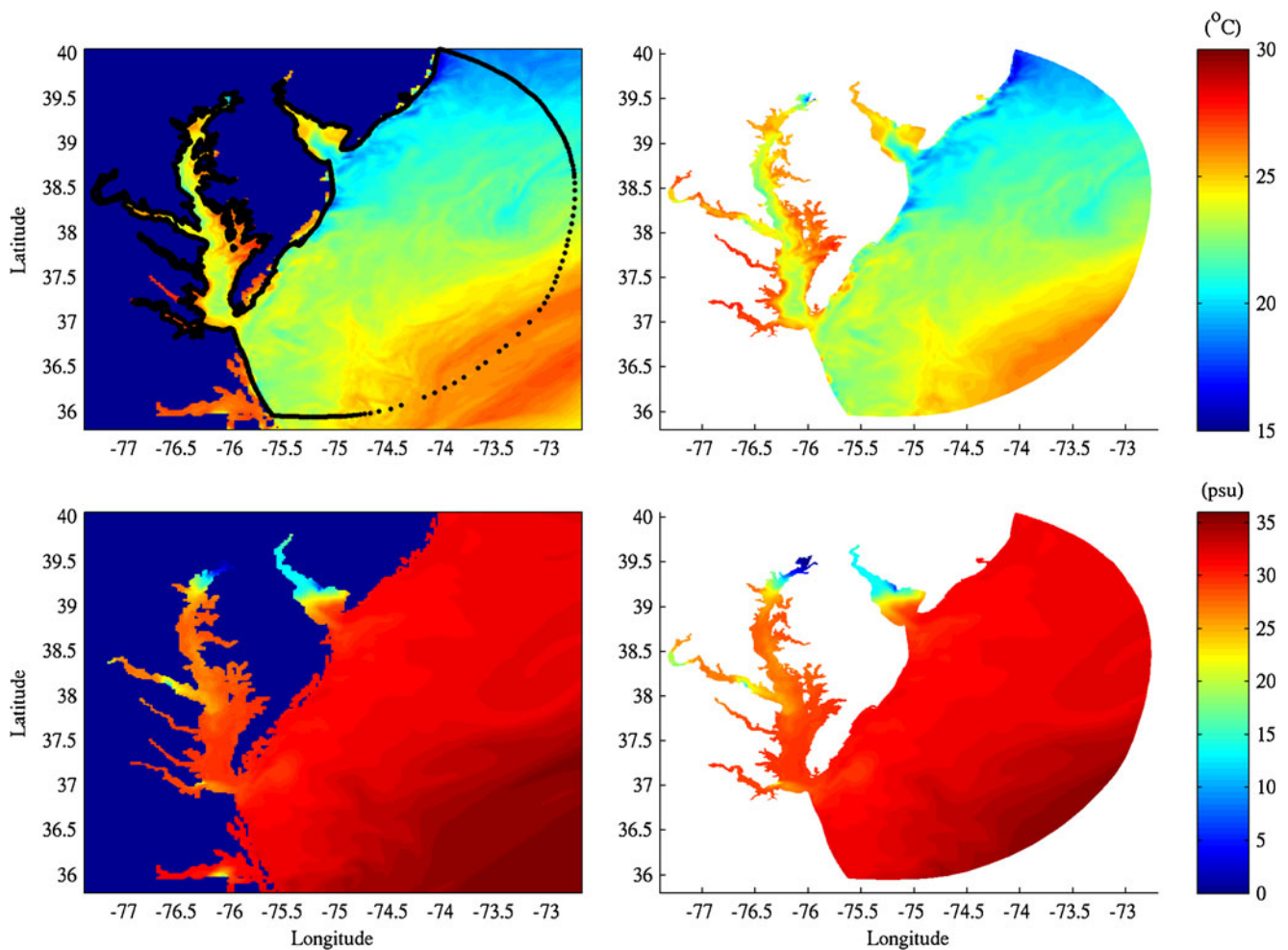


Fig. 9 The NCOM prediction (*left*) of temperature (*top*) and salinity (*bottom*) and the corresponding initial state for the ADCIRC model (*right*) on 3 June 2010

interpolated to the generalized, stretched coordinate native to the ADCIRC model.

The surface temperature and salinity fields from the regional NCOM model on 3 June 2010 are shown in Fig. 9 (left) alongside the derived initial condition for the baroclinic ADCIRC coastal model (right). Temperature fields are shown in the upper panels and salinity in the lower panels. For reference, the ADCIRC grid boundaries are displayed on the NCOM temperature field in the upper lefthand corner. Careful examination of the transfer of surface temperature and salinity data to the coastal model reveals a decent correspondence between the shorelines of the two grids and a successful interpolation of both temperature and salinity features onto the unstructured mesh of the ADCIRC model. While not particularly influential to our region of the study area, strong freshwater gradients in salinity within this initialization field are evident in the upper Chesapeake and Delaware bays. A more rele-

vant feature is the freshwater (yellow) plume signature in the interpolated salinity field entering from the mouth of the James River, just west of the Norfolk Naval Station, and exiting the southernmost portion of Chesapeake Bay mouth onto the shelf. Otherwise, very little variability in the initial salinity field is evident in the local region of interest. In contrast, surface temperature just in the study area exhibits 2–3° of variation in and around the mouth of Chesapeake Bay with cooler waters tracing their origin to the main axis of Chesapeake Bay.

To consider the influence of spatial resolution of the regional model on forecast currents at Cape Henry, a second implementation of the regional model, NCOM, having spatial resolution of 1 km, is configured and applied. This source for initial and boundary conditions is labeled “Relo.” For these comparisons, the boundary frequency is returned to the original 24-h frequency, and tides are applied directly to the coastal model,

ADCIRC, using the FES2004 global tidal database. A comparison of currents computed using initial conditions from the 3- and 1-km resolution NCOM regional models are shown in Fig. 10 and compared to currents measured at Cape Henry. The current predictions at Cape Henry are similar whether the 1- (Relo) or 3-km (Reg) resolution NCOM model is used for initialization and boundary forcing. The spatial resolution of the regional model and its representation of temperature and salinity features is not a source of significant error with regard to current prediction. That is not to say that the regional model effectively represents the underlying and evolving density structure of the region.

At Chesapeake Bay Bridge Tunnel station, Fig. 11 displays a time series of the measured surface temperature (blue) compared to the computed surface temperature from the regional NCOM model (green) and the predicted surface temperature from the coastal model, ADCIRC (red), for the period including 3–6 June 2010. Strong temperature drops of 5° on 3 June and early on 5 June as well as lesser events occurring late on 4 June are indicative of wind-induced upwelling. The regional model temperature shadows these events but with temperature magnitude changes that are a fraction of those associated with the measured values and at times are anti-correlated with the observed temperature trends. The regional model time series is based on hourly NCOM fields. Reinitialization of the coastal model at the beginning for each forecast cycle using daily NCOM fields results in further degradation of the temperature variability as compared to the observed. This is clearly reflected in the smooth and slowly varying temperature values associated with the coastal model. The heat

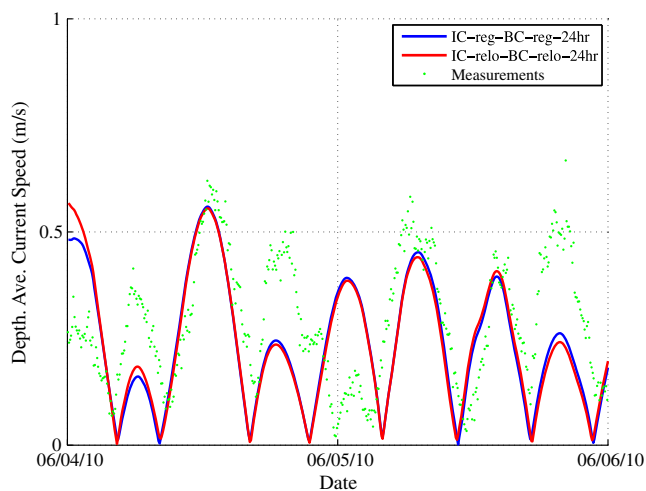


Fig. 10 The effect of regional model spatial resolution on current predictions at Cape Henry

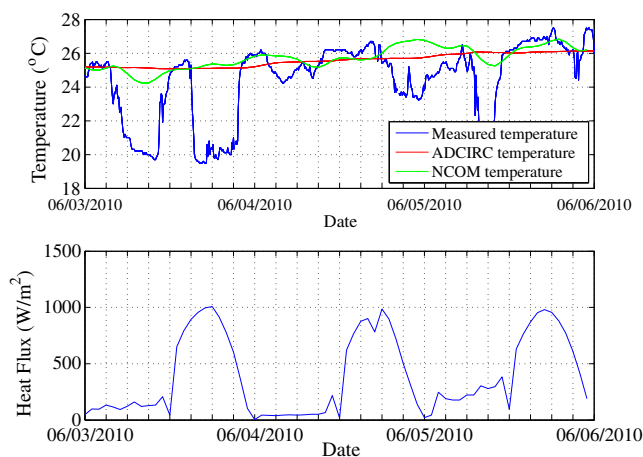


Fig. 11 The measured (blue) and modeled temperature predictions (hourly regional NCOM (green) and ADCIRC (red)) between 3 and 5 June 2010 at the Chesapeake Bay Bridge Tunnel station

flux applied to the coastal model, shown in Fig. 11 and computed internally using surface radiation, latent, and sensible heat fluxes from the COAMPS model, follows an expected diurnal cycle of daylight heating and nighttime cooling and is not likely responsible for the observed temperature pattern. Rather the wind appears to be the dominant force in modifying surface temperature. Blain et al. (2009) have also shown that poor representation of the density structure within the initial condition can be difficult to overcome within the prognostic calculations of the coastal model. While errors in the density structure forecast by the coastal model are expected to persist based on the inadequacy of the regional model initialization and infrequency of the updates, density variability is not the primary driver of the coastal currents in the study region. Rather, wind forcing seems to be the largest modifier of the local coastal dynamics.

5 Evaluation of the tidal response

Hallock et al. (2003) describe the tidal environment as dominated by the M_2 semi-diurnal tide (about 60% of the signal). To isolate the tidal response of the model, the two-dimensional, barotropic mode of the baroclinic ADCIRC model is applied over the same Chesapeake Bay domain, forced by the same FES2004 tidal constituents identified in Section 3 (no winds). Harmonic analysis of the 10-day simulation period (4–14 June 2010) allows resolution of the four major tidal constituents, M_2 , S_2 , K_1 , and O_1 . These modeled tides are compared to NOAA predicted tides at the

Table 6 Harmonic analysis results for June 2010/water level amplitude (centimeters)

Tidal constituent	ADCIRC no winds (cm)	ADCIRC 27-km winds (cm)	ADCIRC 3-km winds (cm)	NOAA predictions (cm)	ADCIRC-NW vs. NOAA (%)	ADCIRC-27 km W vs. NOAA (%)	ADCIRC-3 km W vs. NOAA (%)
K_1	6.48	6.72	5.81	5.8	11.7	15.9	0.2
O_1	4.88	5.10	5.14	4.5	8.4	13.3	14.2
M_2	37.02	36.81	36.67	38	-2.6	-3.1	-3.5
S_2	7.57	8.22	7.65	6.9	9.7	19.1	10.9

Chesapeake Bay Bridge Tunnel station for the same time period. Tidal constituent amplitudes for ADCIRC computed and NOAA predicted tides are presented in columns 2 and 5, respectively, of Table 6. Indeed the M_2 signal is 66% of the total simulated tidal elevation which compares favorably to 68% of the NOAA predicted tide level. Within Table 6, the largest amplitude error, greater than 10%, is associated with the primary diurnal component, K_1 . Tidal elevation phase differences, shown in Table 7 for the model (column 2) and NOAA predictions (column 5), are minor for the semi-diurnal constituents, having values of 5° or less. For O_1 , phase errors are somewhat enhanced but the largest phase errors (approximately 10°) are associated with the dominant diurnal component, K_1 . This initial analysis indicates that within the baroclinic model forecasts, the semi-diurnal tidal frequencies are represented with a significant degree of fidelity. In contrast, replication of the primary diurnal component, K_1 , which comprises nearly 11% of the total tidal signal, may be more challenging.

By adding surface wind forcing to the tidal predictions, the role of wind in the tidal response of the coastal waters can be explored. For the June 2010 forecast period, ADCIRC model simulated water levels subject to tides and wind forcing are obtained using winds of different spatial resolutions (27 vs. 3 km). The tidal constituent analyses and associated comparisons of the modeled tides to the NOAA predicted tides are found in Tables 6 and 7 for tidal amplitude and phase, respectively. When using the 27-km resolution wind forcing, the magnitude of the K_1 tide is amplified over those for the tide-only simulation, leading

to errors on the order of 16%. Upon the application of higher-resolution (3-km) winds, amplitudes for K_1 drop, matching the NOAA predicted values to within 0.2%. The semi-diurnal, S_2 , tide also experiences a reduction in amplitude that lowers the error by more than 8 percentage points. The similarity in strength of these two tidal constituents (K_1 and S_2) may indicate that they are both affected by an increase in the frictional boundary layer due to stronger wind features represented by the more highly resolved wind field. The higher-resolution winds do not have a notable effect on the dominant M_2 tide nor on the phases of any of the constituents.

While the analysis of a single 10-day period in June of 2010 is valuable, a long time series of data such as the hourly sea level variations observed during the Chesapeake Bay Outfall Plume Experiment (COPE-I) (Shay et al. 2001) will provide a more definitive analysis. A second application of the two-dimensional, barotropic mode of the baroclinic ADCIRC model with tidal forcing only is executed from 1 January through 10 October 1996 spanning the dates of the COPE-I experiment to facilitate a comparison. The model domain remains identically the same and forced by the tidal constituents extracted from the FES2004 database but relevant to the 1996 time period. The ADCIRC model solution is decomposed via harmonic analysis into the primary tides, four diurnal and four semi-diurnal constituents, at the location of the NOAA Chesapeake Bay Bridge Tunnel station. The amplitudes and phases of these eight constituents (K_1 , O_1 , Q_1 , P_1 , M_2 , S_2 , N_2 , and K_2) for the COPE-1 measurements, the NOAA harmonic constants reported by NOS (2011), and the

Table 7 Harmonic analysis results for June 2010/water level phase (degrees)

Tidal constituent	ADCIRC no winds (cm)	ADCIRC 27-km winds (cm)	ADCIRC 3-km winds (cm)	NOAA predictions (cm)	ADCIRC-NW vs. NOAA (%)	ADCIRC-27 km W vs. NOAA (%)	ADCIRC-3 km W vs. NOAA (%)
K_1	196.0	197.8	199.0	184.9	6	7	7.6
O_1	202.4	202.5	201.9	208.9	-3.1	-3.1	-3.4
M_2	21.1	21.7	21.7	21.0	0.5	3.3	3.3
S_2	43.4	42.1	44.4	45.8	-5.2	-8.1	-3.1

Table 8 Harmonic analysis results for 1 January–10 October 1996/water level amplitude (centimeters)

Tidal constituents	COPE (1996) (cm)	NOAA predictions (cm)	ADCIRC results (cm)	ADCIRC vs. COPE (%)	ADCIRC vs. NOAA (%)
K_1	5.1	5.8	6.5	27.5	12.1
O_1	4.6	4.5	4.8	4.4	6.7
P_1	2.1	1.8	2.1	0	16.7
Q_1	1.8	0.9	1.1	−38.9	22.2
M_2	37.5	38	37	−1.3	−2.6
S_2	6.8	6.9	7.3	7.4	5.8
N_2	8.4	9	8.8	4.8	−2.2
K_2	2	1.9	1.7	−15	−10.5

ADCIRC computed values are recorded in Tables 8 and 9, respectively. Also included in Tables 8 and 9 are the percent errors (forecast model minus observed value) computed with respect to the observed value (COPE-1 or NOAA). Model predictions again confirm dominance of the M_2 constituent (55% for COPE data, 55% for NOAA predictions, and 53% for ADCIRC) and semi-diurnal constituents generally in the vicinity of the entrance to Chesapeake Bay. While elevation amplitude errors for the ADCIRC model predictions of the semi-diurnal constituents typically average 4% (with the exception of 10–15% errors for K_2) and are less than 2% for the dominant M_2 tide, elevation amplitude errors are appreciably larger for the diurnal constituents (on the order of 12–39%). Tidal elevation phase errors for all constituents are less than 10% but exhibit far greater variability according to the source of the observation, NOAA vs. COPE-I. Notably, errors are largest when compared to COPE-I observations which include the influence of wind. In their analysis of the tidal time series, Shay et al. (2001) suggest that a significant increase in sea level heights during the latter portion of the time series was correlated to frontal passages, i.e., wind dominance. Though winds for the 9-month period in 1996 are not available, 27-km winds can be applied to an analogous 9-month simulation in 2009. Results from a harmonic analysis of that long

time series wind and tide-forced simulation reinforce that the application of winds appears to enhance the K_1 amplitude while little change is observed in tidal amplitudes of the remaining constituents. The tidal phases are unchanged for all constituents when wind forcing is added. These findings reinforce the results of the June 2010 analysis.

Shay et al. (2001) also publish harmonic results from one of the upward-looking acoustic Doppler current profilers (ADCPs) deployed as part of the COPE-I experiment. The ADCP located at (36°52.1' N, 75°47.2' W) recorded three-dimensional velocity vectors at 1-min intervals in 1-m bins starting 3 m above the bottom at a depth of 13.6 m. The first usable data were below the water surface at 1.5 m depth. The 9-month time series began 17 September 1996. Tidal ellipse parameters for the M_2 tidal constituent computed from the ADCP measurements are compared to that of the modeled tidal currents; depth-averaged quantities are recorded in Table 10. The model predicted major current axis for the M_2 tide is within 2.3 cm/s of the observed value. Though the minor axis error is only 1.5 cm/s, relative to its magnitude, this error is rather large. However, the small minor axis also indicates essentially rectilinear tidal variation which decreases the importance of the minor axis. The orientation of the current direction is quite accurate with an error of less

Table 9 Harmonic analysis results for 1 January–10 October 1996/water level phase (degrees)

Tidal constituents	COPE (1996) (deg)	NOAA predictions (deg)	ADCIRC results (deg)	ADCIRC vs. COPE (%)	ADCIRC vs. NOAA (%)
K_1	187.7	184.9	196.2	4.5	6.1
O_1	186.6	208.9	201.6	8	−3.5
P_1	196.7	188.1	197.5	0.4	5
Q_1	172.3	191.1	171.4	−0.5	−10.3
M_2	356.8	21	21.2	6.8	0.9
S_2	49	45.8	45.4	−7.4	−0.9
N_2	327.9	1.4	1.6	10.3	14.3
K_2	46	46.4	45.4	−1.3	−2.1

Table 10 Harmonic analysis results for 1 January–10 October 1996/depth-averaged tidal currents

Tidal ellipse parameters	ADCIRC K_1	ADCIRC M_2	COPE M_2	Difference M_2
Major axis (cm/s)	2.6	14.6	16.9	2.3
Minor axis (cm/s)	0.5	1.4	2.9	1.5
Orientation (deg)	−56.2	−61.9	−64.6	−2.7
Phase (deg)	347.7	173.3	163.8	−9.5

than 3° and phase error is less than 10° which can also be considered quite good. Unfortunately, the NOAA ADCP data at Cape Henry for 2010 is too gap-filled during the June forecast period to permit a meaningful harmonic analysis of the primary tide constituents for the current field. In general, the ability of the ADCIRC model to produce realistic tidal dynamics including the currents is well-published, e.g., Defne et al. (2011), Blain et al. (2010), Hench and Luettich (2003), and Blain (1998).

6 Influence of wind resolution

The tidal analysis of Section 5 reinforces the findings of prior studies in the region (Hallock et al. 2003; Johnson 1995; Shay et al. 2001) that wind is one of the primary driving forces for currents in the area. The effect of wind is included in the coastal forecast system as surface forcing. This forcing is derived from operationally available meteorological forecast data produced by COAMPS, which is distributed by the Fleet Numerical Meteorology and Oceanography Center. The operational 10-m wind product appropriate for the vicinity of Norfolk, VA comes from the Western Atlantic (W_Atl) domain and has a temporal frequency of 3 h and a spatial resolution of 27 km.

The magnitude of the 27-km COAMPS wind field on hour 1 of 7 June 2010 is shown in Fig. 12 (top left) for the western north Atlantic shelf near Chesapeake Bay. Magnification of the same wind speed in the local region of interest is displayed in Fig. 12 (top right). The discontinuous (highly pixelated) values and unrecognizable coastline of the 27-km COAMPS data in Fig. 12 (top panels) highlight the low resolution and resulting lack of variability of the wind speed in the region of

interest. The magnitude of the wind remains rather low between 2 and 8 m/s with little variability. The area surrounding the Norfolk Naval Station is not represented at all, and waters just south of the mouth of Chesapeake Bay are covered by only a few COAMPS grid points at the 27-km resolution. In contrast, the coastal circulation model for this same region has element sizes ranging down to 120 m resolution to resolve the shipping channel and nearby coastal geometry. While the coarse-resolution COAMPS model has been shown to capture low-frequency events (Cambazoglu et al. 2010), wind fields of higher spatial resolution tend to improve wind field predictions as well as the ability of the coastal circulation model to capture localized, short-term, high-frequency events.

To investigate the impact of higher-resolution winds on the baroclinic coastal current forecasts, a triple-nested grid is configured for COAMPS focused on the Chesapeake Bay forecast domain. The coarsest resolution grid remains at 27 km matching the resolution of the operational product and is coupled sequentially to medium- and fine-resolution grids of 9 and 3 km, respectively. Wind speeds from the 3-km nest for hour 0100 on 7 June 2010 are shown in Fig. 12 (bottom left) and Fig. 12 (bottom right). The increased detail of the wind speed is obvious for the 3-km resolution COAMPS product when compared to the 27-km resolution product. The presence of a sharp front extending from within Chesapeake Bay to well offshore over deep waters is clearly visible in the 3-km winds and non-existent in the 27-km winds. The spatial variability of the wind field resulting from higher-resolution atmospheric dynamics over the local region of interest is pronounced when comparing Fig. 12 (bottom right) for the 3-km winds to Fig. 12 (top right) for the 27-km winds. The range of the wind speed (2–18 m/s) is also greater for the 3-km wind product since at this resolution the gradients of the frontal boundary are resolved where the highest wind speeds occur. One should note, however, that even the 3-km resolution wind product crudely represents the coastal outline near Naval Station Norfolk and to the south including the cape at Cape Henry. The wind speed variation depicted in Fig. 13 from the 27-km (red) and 3-km (blue) COAMPS predictions as compared to the observed winds supports the observations noted for Fig. 12. The coarse resolution winds track the low-frequency (1–6 days) signal but diffuse the temporal distinctions between individual frontal passages that occur over hourly time scales. The 3-km COAMPS winds contain more realistic high-frequency events though peak winds remain elevated for time periods exceeding those recorded by the measured values.

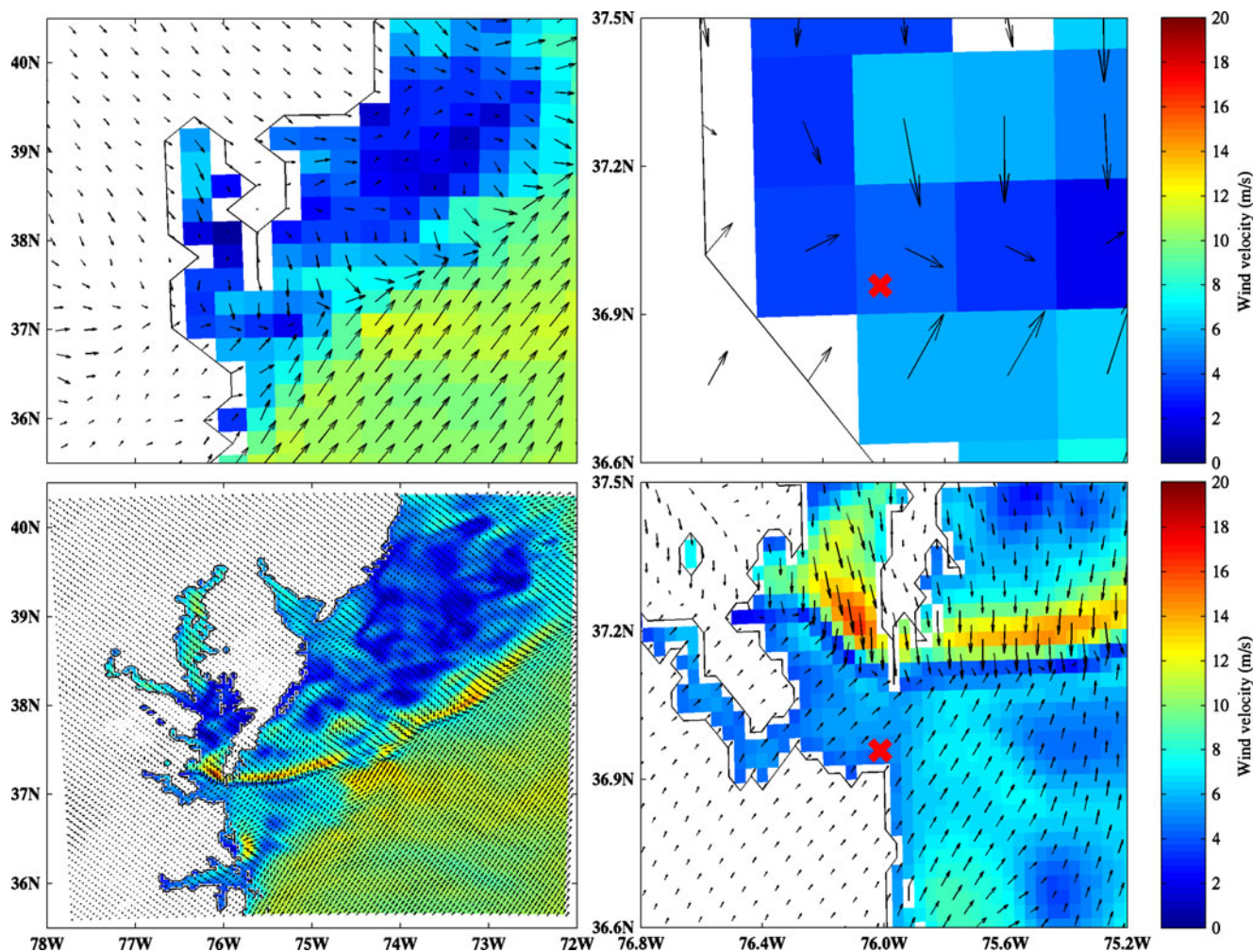


Fig. 12 The magnitude and direction of surface wind at hour 1 on 7 June 2010 from 27-km resolution operational COAMPS over the western North Atlantic shelf (*top left*) and southwest of the Chesapeake Bay, MD (*top right*). Triple-nested, 3-

km resolution COAMPS over the western North Atlantic shelf (*bottom left*) and southwest of the Chesapeake Bay, MD (*bottom right*). The location of the NOAA station at Cape Henry is marked by a *red cross*

Tables 11, 12, and 13 summarize the RMSE, the R^2 , and the Wilmott skill scores associated with the depth-averaged baroclinic currents at stations Cape Henry, Thimble Shoal, and Naval Station Norfolk, respectively, for each 2-day forecast period from 4 to 14 June 2010. Surface wind forcing is derived from the 3-km resolution COAMPS meteorological products. The errors presented can be compared to those in Tables 1, 2, and 3 for current predictions using 27-km winds. Overall the RMSE has decreased and the correlation coefficient has increased for most 2-day forecast periods. Current forecasts during the time from 6 to 8 June were least affected by the increase in resolution of the meteorological forecasts suggesting that other processes dominate the circulation or that the combination of wind direction and still crude representation of the coastline in the meteorological grid combine

to negate any improvements to the forecasts due to resolution alone. The substantial increase in the correlation coefficient with only a modest decrease in the RMSE over the period 4–10 June 2010 indicates that the improved resolution of the wind fields results in better accuracy of the phasing of the currents if not the magnitude.

While improvements to the baroclinic current forecasts are anticipated using a higher-resolution wind product, a quantitative look at the skill of individual model forecasts offers more detailed insight into where and why improvements are realized. Forecasts as described in Section 3 are repeated with the exception that 3-km COAMPS meteorological products are applied as surface forcing. The computed currents for 4–6 June 2010 are shown in Fig. 14 using both coarse and fine-scale winds and compared to observations at

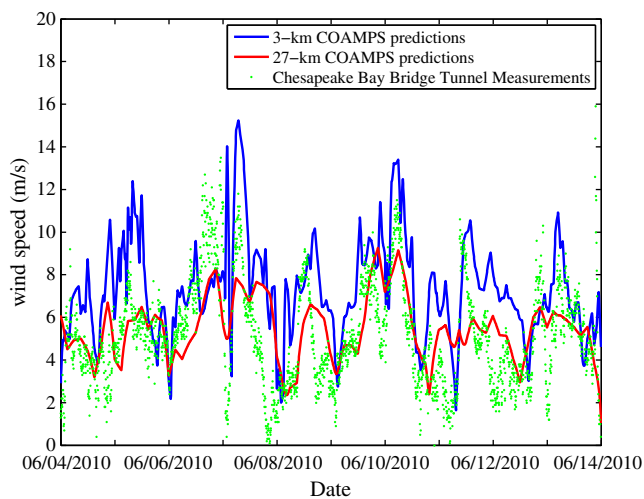


Fig. 13 The wind speed measurements (*green*), 27-km (*red*) and 3-km (*blue*) COAMPS predictions between 4 and 14 June 2010 at the Chesapeake Bay Bridge Tunnel station

all three NOAA ADCP stations, Cape Henry (top), Thimble Shoal (middle), and Naval Station Norfolk (bottom), identified in Fig. 4. At certain times during this initial 2-day period, improvements in the current predictions at Cape Henry using 3-km winds are evident, but fidelity to the observations is inconsistent across tidal cycles. At Thimble Shoal, currents computed using 3- vs. 27-km winds are quite similar showing no advantage to the added resolution, while at the Naval Station Norfolk, modeled currents regardless of wind source show little resemblance to the details of the observed currents. A careful examination of the 3-km wind fields over the inshore stations of Thimble Shoal and Naval Station Norfolk reveal under-resolution of coastal features and lack of detail in the meteorological information similar to the problems noted with the 27-km winds. Clearly, in near-coastal waters with complex shorelines, even a 3-km wind product is insufficient to capture the details needed to force a highly resolved coastal circulation model. As a consequence, the analyses that follow are limited to observations and model forecasts at Cape Henry.

Table 11 Baroclinic current (depth-averaged) error statistics at Cape Henry for 3-km winds

Date	RMSE (m/s)	R^2	Wilmott skill score
4–6 June	0.160	0.481	0.682
6–8 June	0.262	0.507	0.625
8–10 June	0.144	0.887	0.929
10–12 June	0.278	0.398	0.640
12–14 June	0.256	0.586	0.746

RMSE root mean square error, R^2 correlation coefficient

Table 12 Baroclinic current (depth-averaged) error statistics at Thimble Shoal for 3-km winds

Date	RMSE (m/s)	R^2	Wilmott skill score
4–6 June	0.140	0.197	0.486
6–8 June	0.172	0.271	0.562
8–10 June	0.227	0.040	0.427
10–12 June	0.233	−0.038	0.365
12–14 June	0.258	0.086	0.413

RMSE root mean square error, R^2 correlation coefficient

The set of model forecast baroclinic currents (shown as depth-integrated) subject to 27-km (red) and 3-km (blue) wind forcing for 4–14 June 2010 are compared to observed (also depth-integrated) currents at Cape Henry in 2-day increments. Depicted along with the currents are feather plots of the applied wind magnitude and direction for both the 27- and 3-km resolution wind fields. The 2-day period from 4–6 June 2010 is presented in Fig. 15 and the remaining 2-day forecast periods are depicted in Fig. 16 for 6–8 June 2010, Fig. 17 for 8–10 June 2010, Fig. 18 for 10–12 June 2010, and Fig. 19 for 12–14 June 2010.

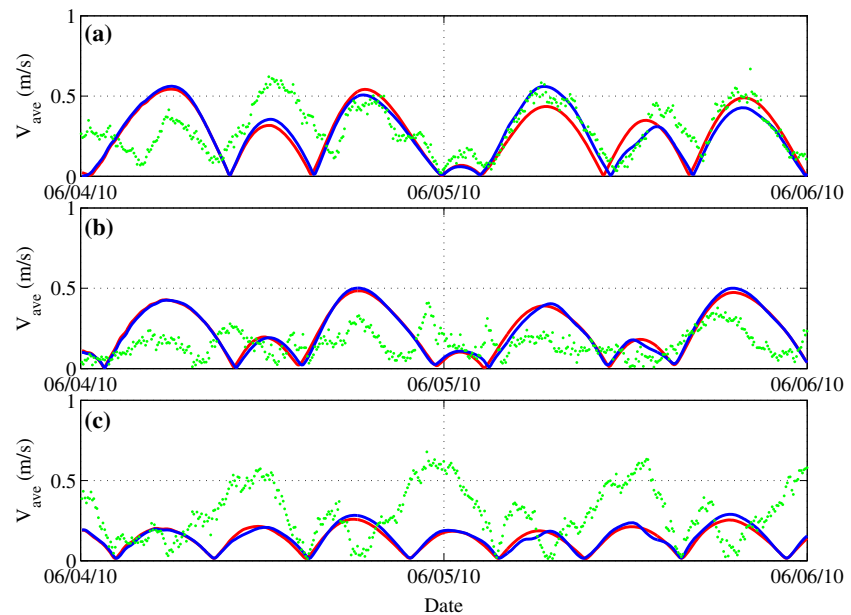
For the 4–6 June 2010 time frame (Fig. 15), winds vary substantially in both magnitude and direction between the 3- and 27-km resolution products. The modeled currents tend to exhibit larger deviations from the observed currents for certain wind directions. Between 3 and 16 h on 4 June, winds are from the south-southwest. During this time, predicted currents are both over- and underpredicted as compared to the observations and exhibit only small changes in response to the differing wind resolution. Once the winds shift direction and come from the north around 1800 hours June 4 and again after 0300 hours June 5, current predictions better reflect the measured currents. Though not perfect, a much better adherence to the phasing of the ebb and flood currents is evident with the higher-resolution winds. During 6–8 June 2010 (Fig. 16), both wind fields generally maintain the same wind direction

Table 13 Baroclinic current (depth-averaged) error statistics at Naval Station Norfolk for 3-km winds

Date	RMSE (m/s)	R^2	Wilmott skill score
4–6 June	0.236	0.120	0.448
6–8 June	0.223	−0.005	0.425
8–10 June	0.216	0.010	0.414
10–12 June	0.275	0.236	0.473
12–14 June	0.279	0.173	0.448

RMSE root mean square error, R^2 correlation coefficient

Fig. 14 Forecasts of baroclinic current magnitude (depth-averaged) at Cape Henry (*top*), Thimble Shoal (*middle*), and Naval Station Norfolk (*bottom*) for 4–6 June 2010 using 27-km (*red*) and 3-km (*blue*) resolution surface winds compared to NOAA observed currents (*green dots*)



but the 3-km winds have nearly three times the magnitude of the 27-km wind stress at their peak (with the exception of a period from 1500 hours 6 June to 0000 hours 7 June during which the 27-km wind stresses exceed those of the 3-km winds). Currents forced by 3-km winds tend to have a better representation of the current magnitude profile, something particularly evident in the first 12–18 h on 7 June. With the passage

of the strong front moving from the north to the south over Chesapeake Bay (seen in Fig. 12 for 0100 hours on 7 June 2010), a large displacement of fresh water may be pushed out of the bay. This phenomena will only be realized in the coastal model if the initial conditions from the regional model reflect these changes in the density field, which is unlikely given the even coarser (NOGAPS 0.5°) source of atmospheric forcing applied

Fig. 15 Two-day model forecasts of baroclinic currents compared to observed currents (*green*) (both depth-averaged) from 4 to 6 June 2010 together with the applied COAMPS wind magnitude and direction from the 27-km (*red*) and 3-km (*blue*) resolution products

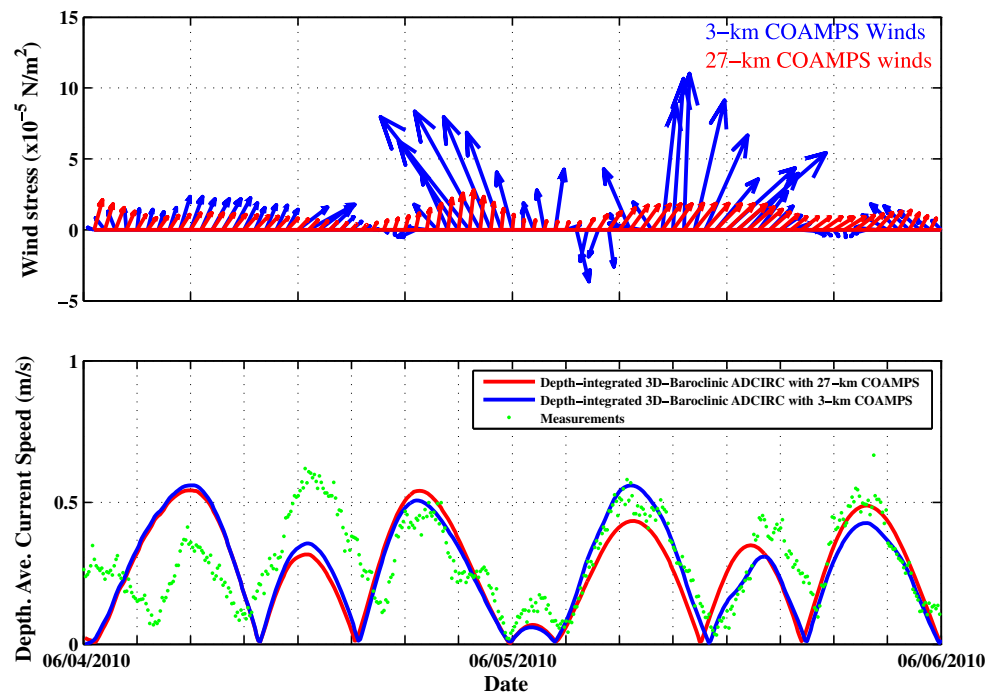
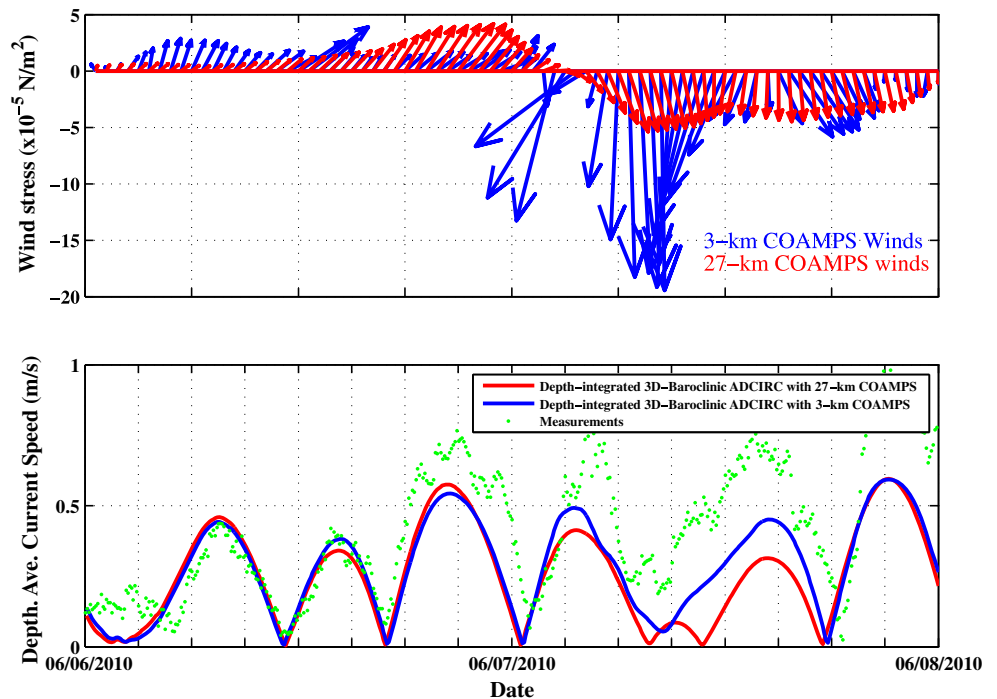


Fig. 16 Two-day model forecasts of baroclinic currents compared to observed currents (*green*) (both depth-averaged) from 6 to 8 June 2010 together with the applied COAMPS wind magnitude and direction from the 27-km (*red*) and 3-km (*blue*) resolution products



to the regional model. Recall that the coastal model implementation for Chesapeake Bay does not include additional fresh water influx. The 2-day forecasts for currents from 8 to 10 June 2010 (Fig. 17) exhibit similar trends as those discussed for the previous two forecast periods (4–8 June). The final two forecast periods, 10–12 June and 12–14 June 2010 shown in Figs. 18 and 19,

respectively, demonstrate that when winds are predominately from a southerly direction (SW-S-SE), the wind resolution has little effect on the current predictions.

The issue of predicted current accuracy and the relation to wind direction deserve additional attention. Considering the period 4–14 June 2010, several current profiles are selected to represent times of differing wind

Fig. 17 Two-day model forecasts of baroclinic currents compared to observed currents (*green*) (both depth-averaged) from 8 to 10 June 2010 together with the applied COAMPS wind magnitude and direction from the 27-km (*red*) and 3-km (*blue*) resolution products

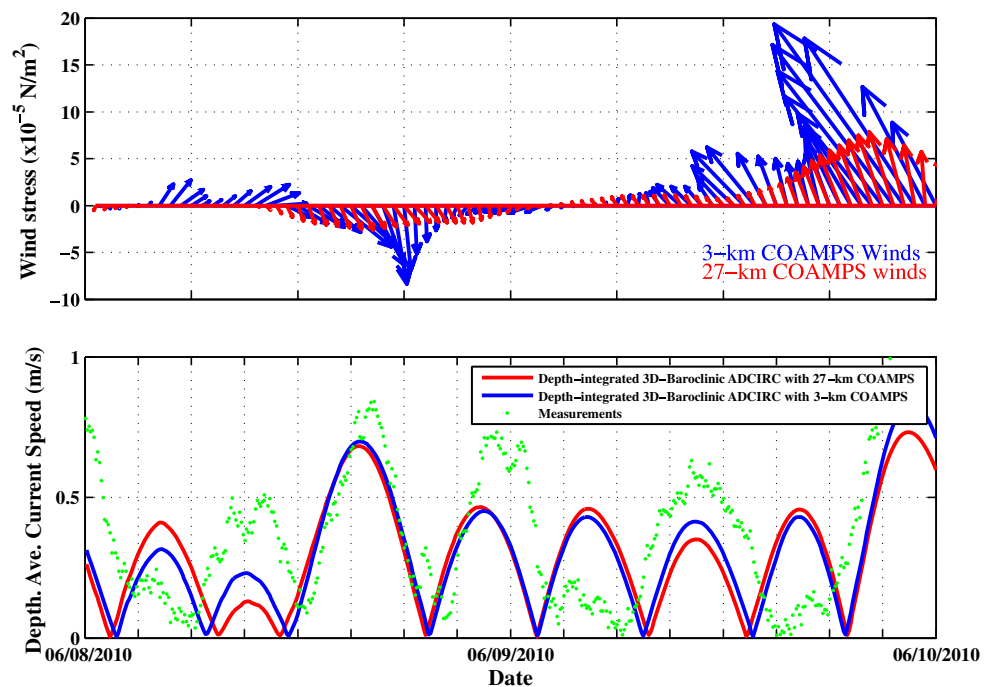
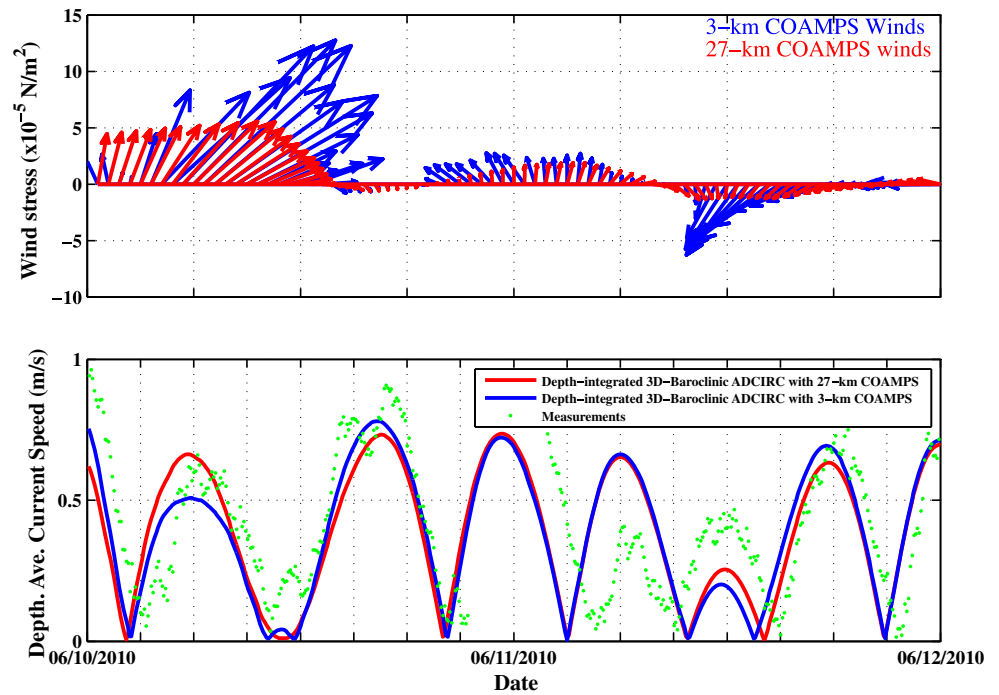


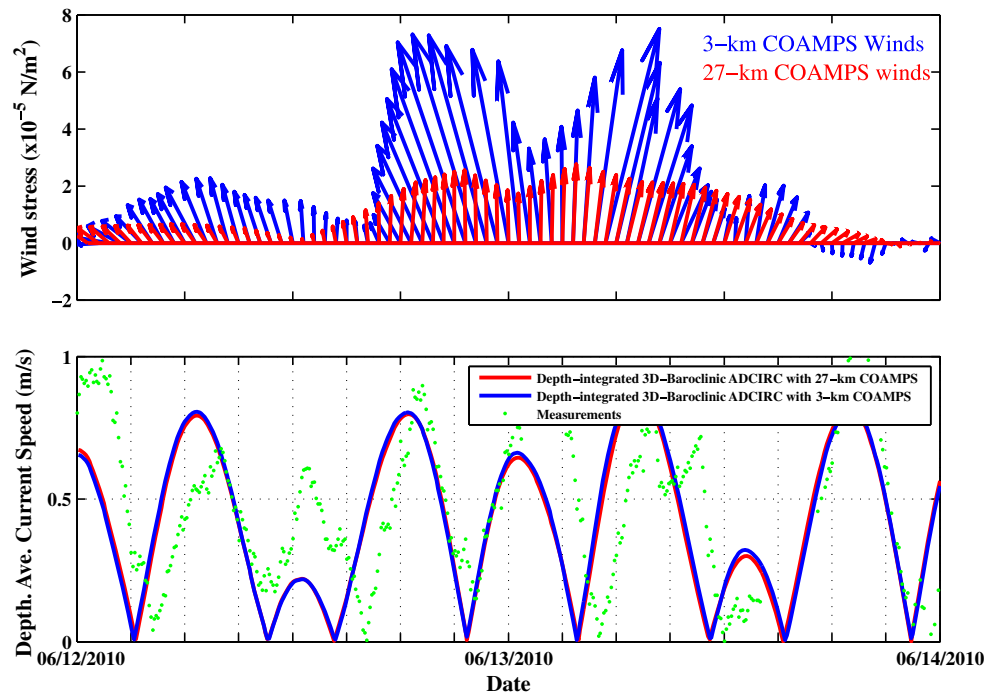
Fig. 18 Two-day model forecasts of baroclinic currents compared to observed currents (*green*) (both depth-averaged) from 10 to 12 June 2010 together with the applied COAMPS wind magnitude and direction from the 27-km (*red*) and 3-km (*blue*) resolution products



direction. These currents (using both 3- and 27-km winds) are compared to the measured currents over the water column at Cape Henry. Figure 20 presents the horizontal current magnitude for 4 June at 1900 and 2200 hours and 5 June at 0600, 0900, and 1200 hours. These times correspond to winds from the NE, SE, NW, S, and SW, respectively. At times when winds are from

the NE, NW, or S, the model currents align well with the observed currents from 7.5 m depth down to 18 m depth. From Fig. 20, model depth is 2 m shallower than the depths recorded at Cape Henry. The result is that currents in the bottom boundary layer of the model (the final 1 m) are significantly reduced in magnitude over the measured values. The mismatch of simulated

Fig. 19 Two-day model forecasts of baroclinic currents compared to observed currents (*green*) (both depth-averaged) from 12 to 14 June 2010 together with the applied COAMPS wind magnitude and direction from the 27-km (*red*) and 3-km (*blue*) resolution products



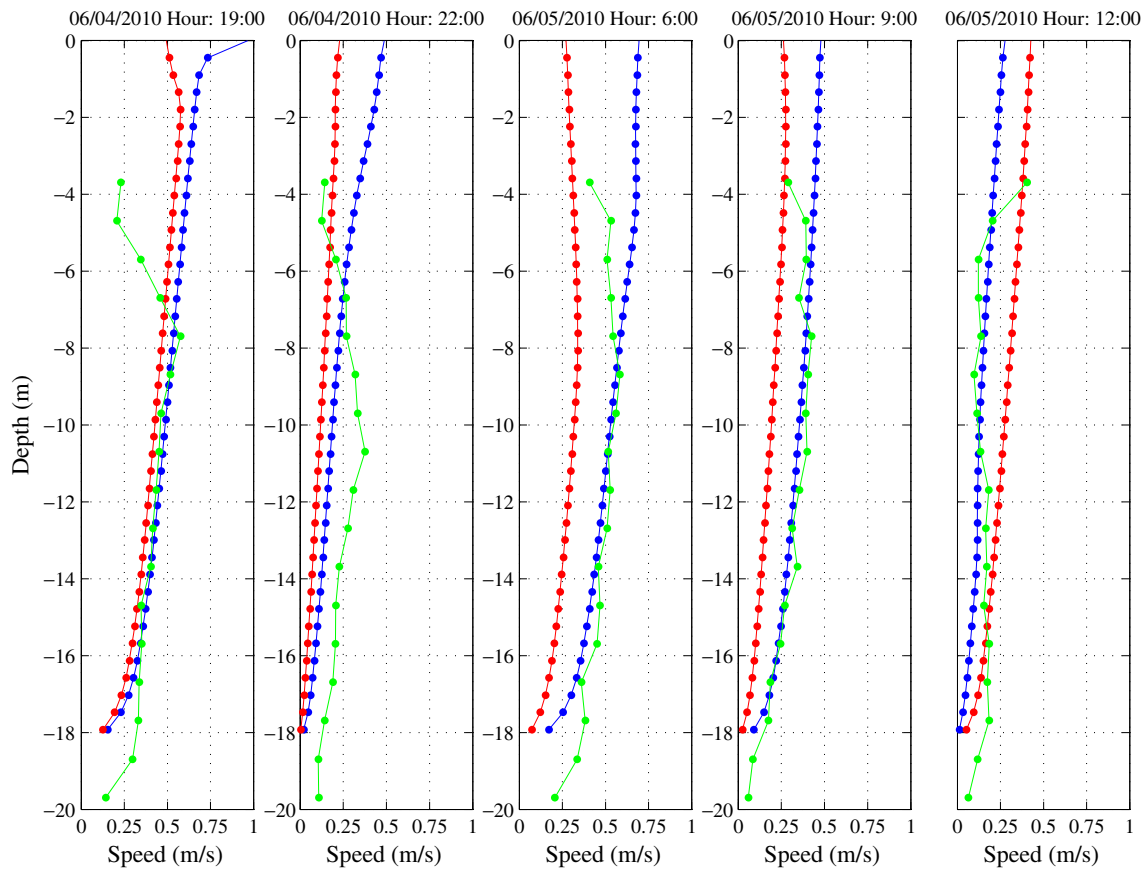


Fig. 20 Magnitude of the horizontal current modeled using 3-km winds (blue) and 27-km winds (red) vs. the observed values (green) on 4 June 2010 at 1900 hours and 2200 hours and on 5 June 2010 at 0600 hours, 0900 hours, and 1200 hours

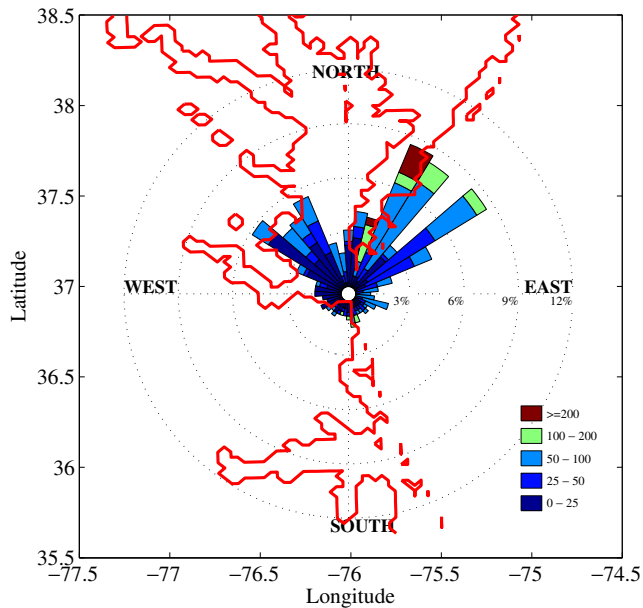


Fig. 21 A wind rose located at Cape Henry for 4–6 June 2010 depicting frequency of occurrence (in percent) and magnitude of the current error (color). The shoreline from the 3-km COAMPS is depicted in red

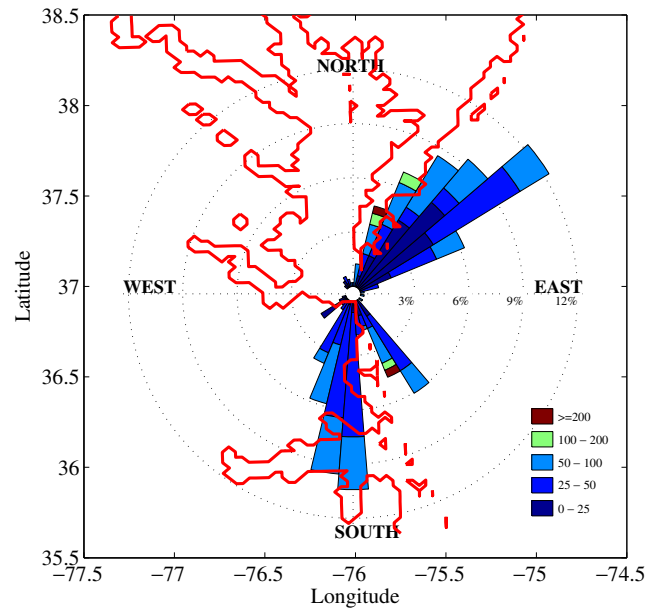


Fig. 22 A wind rose located at Cape Henry for 6–8 June 2010 depicting frequency of occurrence (in percent) and magnitude of the current error (color). The shoreline from the 3-km COAMPS is depicted in red

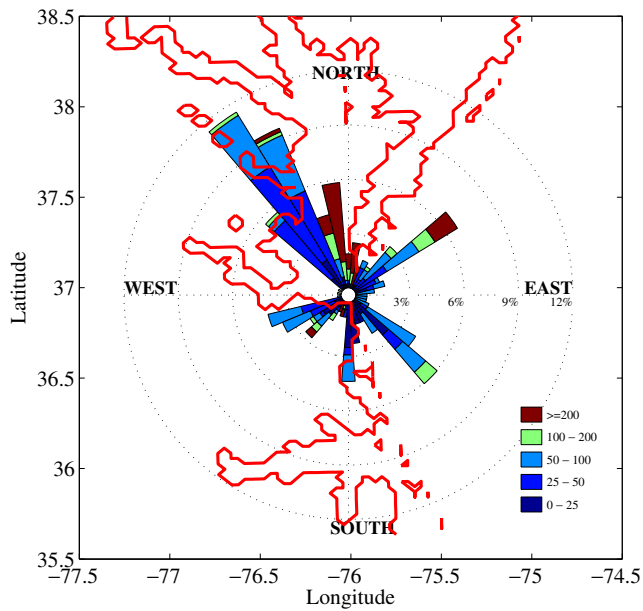


Fig. 23 A wind rose located at Cape Henry for 8–10 June 2010 depicting frequency of occurrence (in percent) and magnitude of the current error (*color*). The shoreline from the 3-km COAMPS is depicted in *red*

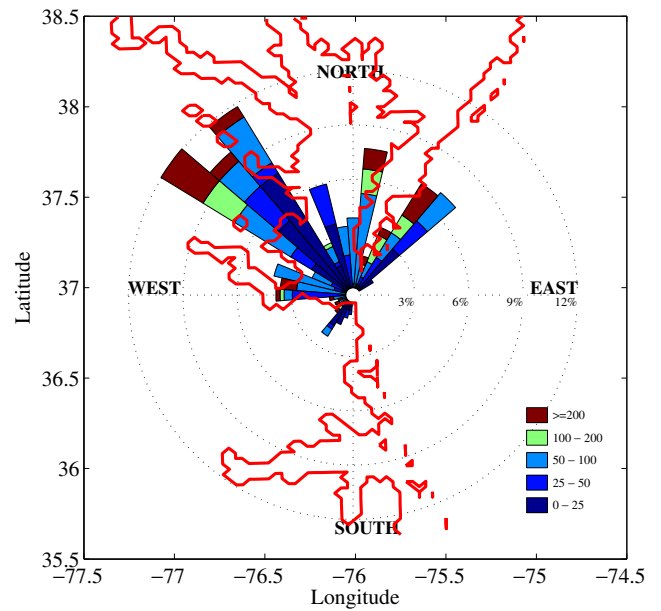


Fig. 25 A wind rose located at Cape Henry for 12–14 June 2010 depicting frequency of occurrence (in percent) and magnitude of the current error (*color*). The shoreline from the 3-km COAMPS is depicted in *red*

currents above 7.5 m when compared to measured values may be due to a lag in the model response to the changing wind direction. Each of the times selected occurs with a wind direction change. Current profiles

that have winds from the same direction for several hours (not shown) show better agreement in the surface layer with observations. In general, however, the magnitude of the surface currents is not well captured

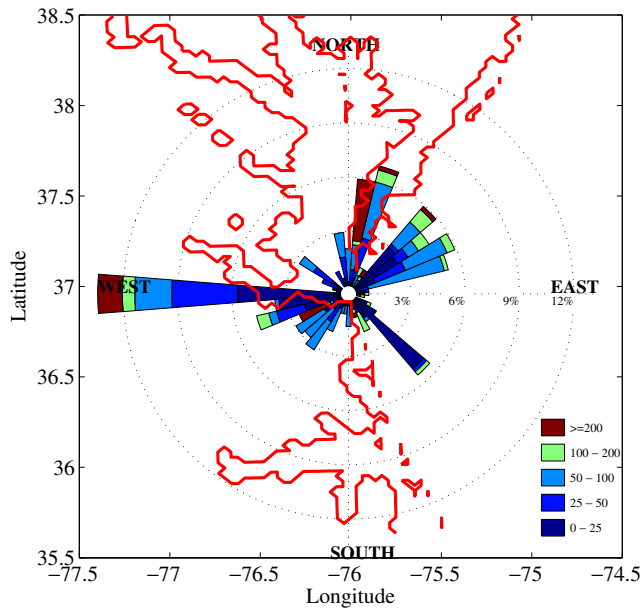


Fig. 24 A wind rose located at Cape Henry for 10–12 June 2010 depicting frequency of occurrence (in percent) and magnitude of the current error (*color*). The shoreline from the 3-km COAMPS is depicted in *red*

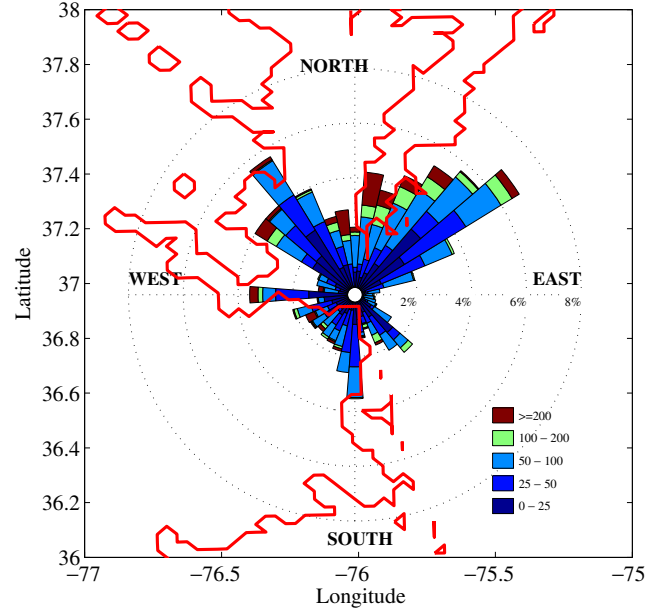


Fig. 26 A wind rose located at Cape Henry for 4–14 June 2010 depicting frequency of occurrence (in percent) and magnitude of the current error (*color*). The shoreline from the 3-km COAMPS is depicted in *red*

by the model. Based on recent work in storm surge applications (Westerink et al. 2008), the marine response to the winds is shown to be strongly modified by surface drag that varies due to the coastal canopy and land use, among other things. These effects have not been accounted for in the configured forecast system.

To quantify the heuristic observations highlighted in Fig. 20, diagrams representing direction of the wind vector at Cape Henry (shown in context of a compass rose), frequency of occurrence of a specific wind direction (length of ray from center in percent), and magnitude of the resulting depth-averaged current error (color bar) are constructed and presented in context of the COAMPS 3-km resolution coastal outline (red) in Figs. 21, 22, 23, 24, and 25 for five 2-day forecasts and in Fig. 26 for the 10-day period from 4 to 14 June 2010. The current error is a percent absolute error when compared to the observed currents. During the 4–6 June 2010 period (shown in Fig. 21), the most

frequently occurring wind comes from the SSW, SW, and WSW directions. The SSW and SW winds at Cape Henry that pass directly over land with minimal marine fetch are associated with the largest current error. Over the next 2 days, 6–8 June winds (shown in Fig. 22) are predominately from the WSW or the north. These winds are well-resolved by the 3-km COAMPS model resulting in notably less error in the computed currents. Errors are again evident in the currents associated with a SSW wind. From 8 to 10 June (shown in Fig. 23) winds are varied with most coming from the SE. These wind-forced currents have lower error. However, if the wind shifts to originate from a SSE or southerly direction, the winds pass over the N–S oriented coastline south of Cape Henry and result in fairly large current errors. On June 10 (shown in Fig. 24), a large wind event blows in from the SSW creating large errors due to the proximity of land in the COAMPS model. The most frequent wind, though not of great strength, comes from east.

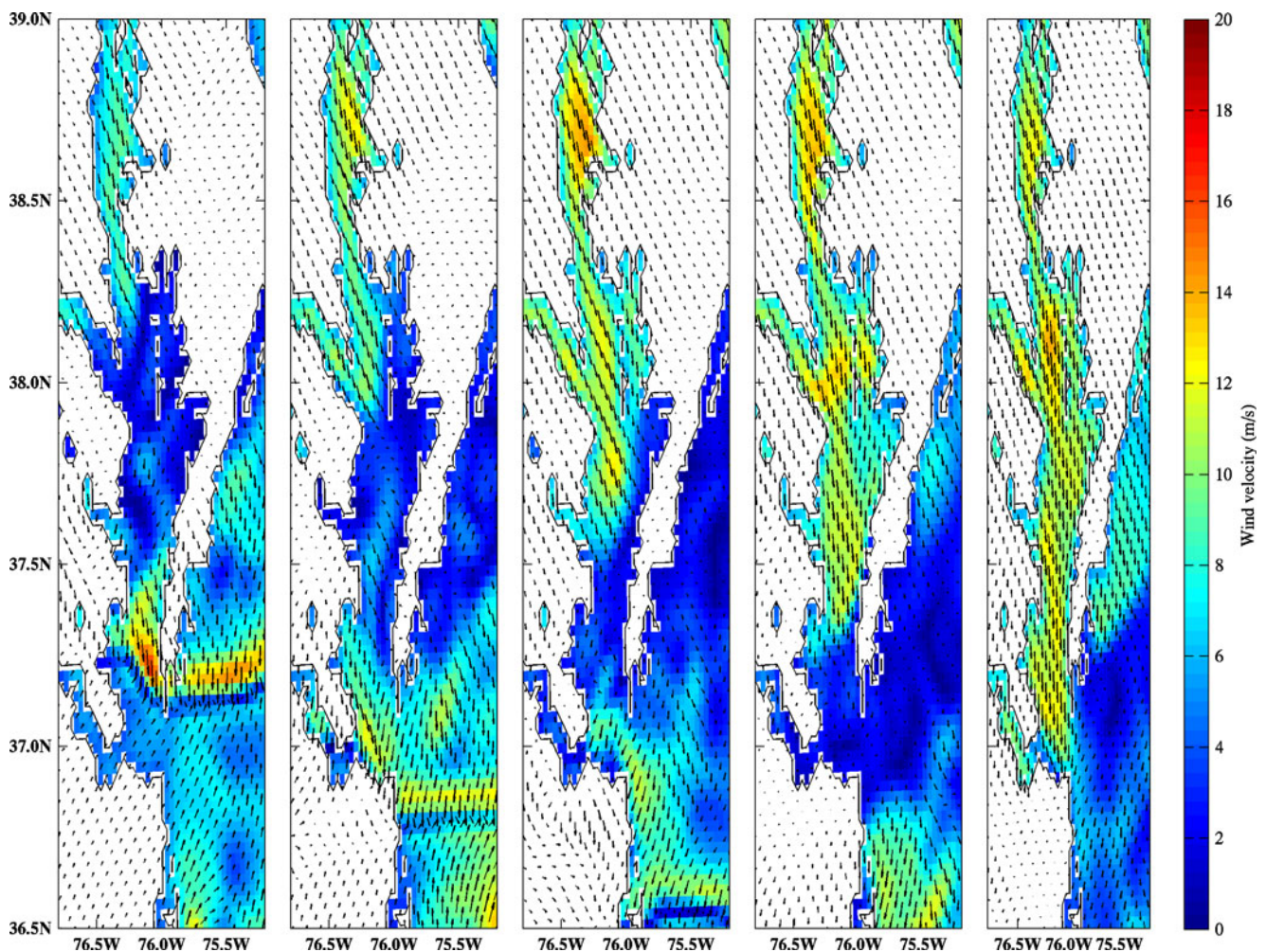


Fig. 27 Magnitudes and directions of the 3-km resolution COAMPS wind over Chesapeake Bay from 0100 to 0500 hours 7 June 2010

This wind follows along the shoreline north of Naval Station Norfolk and produces current error due to the marine wind contamination by the close proximity of the shoreline in the COAMPS model. During the final forecast period (12–14 June shown in Fig. 25), winds are largely from a southerly direction with SE and SSW winds leading to the largest current error. A summary of all winds for the 10-day period (shown in Fig. 26) reinforce that winds at Cape Henry typically originate from the southeast or southwest directions though at times a northerly wind event will occur. Increased current error is nearly always associated with winds that are interacting with the shoreline, that is, winds from the SSW, SSE, and E directions. This finding is supported by the variation of the RMSE and R^2 in Table 11. The highest correlation and lowest RMSE occur during the 2-day forecast periods during which the most frequent winds originate from the SW or SE at an angle that is not influenced by the nearby shoreline. The examination of vertical current profiles in Fig. 20 suggests that improvements to the wind drag applied to winds interacting with the land may result in a reduction of current error.

Errors in the applied wind fields are not limited to insufficient spatial resolution. The frequency of the atmospheric forcing update to the forecast system also becomes important in representing near-coastal and estuarine dynamics. Typical temporal resolution of the operational winds is three-hourly. For 7 June, the 3-km resolution COAMPS is recomputed, saving meteorological fields every hour. COAMPS wind speeds for the first 5 h on 7 June are depicted sequentially in hourly intervals from left to right in Fig. 27. During hour 1, a sharp front has developed over the lower Chesapeake Bay with peak wind speeds of 14–16 m/s. At this same time at Cape Henry, winds are only 4–6 m/s. By the second hour, the strongest winds associated with the front have already passed and moved south of the Cape Henry station resulting in wind speeds that are only 8–10 m/s. The coastal circulation model interpolates between available wind fields, in this case between winds at hour 1 and hour 2, to provide wind forcing at every model time step. The result is that the coastal currents at Cape Henry will never be subjected to the strongest winds associated with the frontal passage but instead will experience winds that are linearly interpolated between 4–6 and 8–10 m/s. A similar situation is observed by comparing wind magnitudes from hour 3 to hour 4. At hour 3, winds at Cape Henry are 8–10 m/s while to the northwest, winds are elevated at 6–8 m/s. These higher winds would be expected to pass over Cape Henry. But at hour 4, there is no evidence of this wind event with wind magnitudes between 0 and

2 m/s. This degradation of the wind forcing caused by temporal resolution is evident when considering hourly fields; the operational wind products that are available only every 3 h would contain even less variability.

7 Conclusions

A coastal forecast system has been designed using a baroclinic unstructured grid model (ADCIRC) as the core simulator. External forcing is derived from a regional model (NCOM) and a mesoscale atmospheric prediction system (COAMPS) that are both globally available. The purpose of this forecast system is the prediction of baroclinic currents at locations worldwide on time scales of hours at resolutions of 100–200 m in near-coastal waters. These type of environments are subject to the full range of wind, tide, and density-driven dynamics; have shallow and highly variable bathymetry; and are adjacent to convoluted shorelines. The accurate prediction of currents depends on an appropriate configuration of all aspects of the forecast system. The purpose here is to better understand the performance of such a forecast system and identify the primary sources of error that result in degraded or inconsistent fidelity in the prediction of baroclinic coastal currents.

For this purpose, the coastal forecast system is applied to a localized region in the southwest corner of Chesapeake Bay, near Norfolk Naval Station, Norfolk, VA. Navigation and military exercises in nearby waters necessitate environmental knowledge of the currents. Furthermore, real-time observations of currents and water level are available. A series of baroclinic current forecasts were performed for 4–14 June 2010 and subsequently analyzed to determine not only the performance of the forecast system as configured but also the source(s) of current error. To this end, various dynamical components of the forecast coastal currents were examined separately including the impact of the regional model forcing, the tidal response, and the influence of wind resolution and direction. The focal point for the analyses are the Cape Henry NOAA ADCP station and the Chesapeake Bay Bridge Tunnel NOAA Water Level station.

The baroclinic current forecasts themselves exhibited considerable variability in RMSE and correlation coefficients for each of the five 2-day periods. At times currents were predicted within 17 cm/s with an average error over the 10-day period of 25 cm/s. Low correlation coefficients (0.38–0.65) when compared to measured currents were indicative of a phase error in the predicted currents. Starting with the influence of the regional model on baroclinic currents, the analysis

did reveal a phase lag error on the order of 90 min to 2 h. The representation of tidal variability at the open ocean boundary is critical to accurate coastal current prediction, yet the prescription of tides at the boundary depends on either high temporal frequency of the regional model boundary forcing (greater than three-hourly) or the application of an external tidal database directly to the coastal model. Spatial resolution of the regional model (1 vs. 3 km) did not appear to impact current predictions at Cape Henry. The density structure of the regional model translates accurately to the coastal model for initialization, but does not exhibit strong density-driven features in the near-coastal regions of interest. In fact, surface temperature comparisons highlight inadequacies in the regional model fields, likely caused by poor wind forcing that then results in too little variability of the surface temperature in the coastal model.

When evaluating the ability of the coastal model to accurately simulate the tidal response, the dominance of the M_2 in water level is reproduced accurately for both the forecast period in June of 2010 and for a 9-month time series in 1996 at the same location where measurements were made as part of the COPE experiment (Shay et al. 2001). Errors in the magnitude of M_2 water level are less than 3 cm, and phase errors are less than 1° . For both datasets, water levels for the K_1 tidal constituent are amplified over measured values by approximately 10%. Upon adding winds (the forecast 27-km winds) to the tidal computations, significant wind events further enhance water levels associated with the primary diurnal tide. Water level phases are unaffected by the addition of wind. Increasing the wind resolution to 3 km leads to marked improvement of the representation of the K_1 tidal constituent, reducing water level errors to 0.2% and leaving the M_2 predictions essentially unchanged. Stronger winds in the 3-km wind field enhance the frictional effects throughout the water column, damping the diurnal constituents. Using the observed currents at the COPE location in 1996 for comparison, the modeled M_2 tidal current is accurately represented considering the major and minor axes (2.3 and 1.5 cm/s error), orientation (2.7° lag), and phase (9.5° lag). In summary, the coastal forecast system is able to accurately predict the dominant tidal response in both water level and currents but only when a more finely resolved wind field (i.e., 3 km in this case) is applied.

The application of higher-resolution (3 km) winds results in an improved representation of high-frequency variations due to frontal passages while the coarse (and fine) resolution winds reproduce the 2–7-day variability quite well. Upon further investigation, application of

the higher-resolution (3-km) COAMPS wind product within the coastal forecast system reduced RMSE for the five 2-day forecast periods down to an average of 21 cm/s and raised the correlation coefficient to a range of 0.40 to 0.89. A breakdown of the current error in relation to the wind direction further reveals that uncertainty in the forecast currents is largely due to error in winds that strongly interact with the shoreline. Winds at Cape Henry originating from the south-southeast, south-southwest, and easterly direction blow parallel to the shoreline which is not well resolved even within 3-km COAMPS products. This is the primary source of error in the current forecasts. Currents are well predicted for winds that originate from other directions. The application of wind drag coefficients that reflect relief of the coastal topography and capture the terrestrial or marine origin of the wind could also improve the wind stress field applied within the coastal forecast system. A brief look at the temporal resolution of the wind field suggests that the three-hourly wind fields and even 1-h wind fields will miss strong frontal passages with the result that currents will not exhibit a response to these important coastal events.

To summarize, surface wind fields serve as a significant forcing mechanism in shallow coastal waters. Spatial resolution of the wind features and of the adjacent shoreline within the meteorological model is critical for accurate prediction of coastal currents. High temporal resolution on the order of hours or less will notably improve the ability of forecast currents to reflect event-driven dynamics which often dominate coastal processes. In analyzing coastal current forecasts, it is important to examine all possible sources of error in detail. In this way, the predictability of the error can better be determined or configuration of the forecast system can be altered to minimize the error source. Initially, the current forecast errors associated with the June 2010 event appeared unpredictable and even random. Upon analysis, times of specific wind directions were identified as error prone while other times and processes yield reliable forecasts. What remains is to investigate the role of friction, freshwater inputs, and wind-induced upwelling on the prediction of currents at inshore coastal stations such as Thimble Shoal and Norfolk Naval Station.

Acknowledgements The authors would like to thank Travis Smith for his work on the COAMPS-NCOM coupled model system which made it possible to create high-resolution wind fields and multiple realizations of the regional model. We appreciate the efforts of Philip Chu whose model–model comparisons in the same region provided the motivation for this study. The work for this paper has been funded under the NRL 6.2 Core Program, “Development of a Multi-Scale Coupled Ocean Model

System—Application to the Turkish Straits.” This paper is NRL contribution number JA/7320–11-0631.

References

- Allard R, Dykes J, Hsu Y, Kaihatu J, Conley D (2008) A real-time nearshore wave and current prediction system. *J Mar Syst* 69(1–2):37–58
- Barron CN, Kara A, Hurlburt H, Rowley C, Smedstad L (2004) Sea surface height predictions from the global Navy Coastal Ocean Model (NCOM) during 1998–2001. *J Atmos Ocean Technol* 21(12):1876–1894
- Barron CN, Kara A, Martin P, Rhodes R, Smedstad L (2006) Formulation, implementation and examination of vertical coordinate choices in the global Navy Coastal Ocean Model (NCOM). *Ocean Model* 11:347–375. doi:10.1016/j.ocemod.2005.01.004
- Blain CA (1998) Barotropic and tidal residual circulation in the Arabian Gulf. In: Spaulding ML, Blumberg AF (eds) Estuarine and coastal modeling, proceedings of the fifth international conference. American Society of Civil Engineers, Reston, pp 166–180
- Blain CA, Preller RH (2007) High resolution modeling of coastal inundation: user requirements and current practice, a navy perspective. *Mar Technol Soc J* 41(1):76–83
- Blain CA, Cambazoglu MK, Kourafalou V (2009) Modeling the Dardanelles strait outflow plume using a coupled model system. In: OCEANS 2009, MTS/IEEE Biloxi—marine technology for our future: global and local challenges, marine technology for our future: global and local challenges. MTS/IEEE, Biloxi, MS, pp 1–8
- Blain CA, Linzell R, Chu P, Massey C (2010) Validation test report for the advanced circulation model (ADCIRC) v45.11. NRL memorandum report NRL/MR/7320-2009-9205. Naval Research Laboratory, Washington, DC
- Blumberg AF, Goodrich DM (1990) Modeling of wind-induced destratification in Chesapeake Bay. *Estuaries* 13:236–249
- Blumberg AF, Mellor GL (1987) Three dimensional coastal ocean models, coastal and estuarine sciences. A description of a three-dimensional coastal ocean circulation model, vol 4. American Geophysical Union, Washington, DC, pp 1–16
- Blumberg AF, Signell RP, Jenter HL (1993) Modeling transport processes in the coastal ocean. *J Mar Environ Eng* 1:31–52
- Burchard H (2002) Applied turbulence modeling in marine waters. Lecture notes in earth sciences, vol 100. Springer, New York
- Cambazoglu MK, Blain CA, Kadioglu M (2010) Evaluation of wind fields predictions by atmospheric models over the Marmara Sea. In: Rapp. comm. int. mer mdit., 39th international CIESM congress, vol 39. CIESM, Venice, Italy, p 99
- Chen C, Liu H, Beardsley RC (2003a) An unstructured grid, finite-volume, three-dimensional, primitive equations ocean model: application to coastal ocean and estuaries. *J Atmos Ocean Technol* 20:159–186
- Chen S, Cummings J, Doyle J, Hodur R, Holt T, Liou C, Liu M, Ridout J, Schmidt J, Thompson W, Mirin A, Sugiyama G (2003b) COAMPS version 3 model description—general theory and equations. NRL Publication NRL/PU/7500–03-448. Naval Research Laboratory, Monterey
- Chu PY, Jacobs GA, Cambazoglu MK, Linzell RS (2011) Multi-model validation in the Chesapeake Bay region in June 2010. *J Mar Syst* (submitted)
- Defne Z, Hass KA, Fritz HM (2011) Numerical modeling of tidal currents and the effects of power extraction on estuarine hydrodynamics along the Georgia coast, USA. *Renew Energy* 36(12):3461–3471. ISSN 0960-1481, doi:10.1016/j.renene.2011.05.027
- Dresback KM (2005) Algorithmic improvements and analyses of the generalized wave continuity equation based model, ADCIRC. Ph.D. thesis, University of Oklahoma, Norman, OK, p 228
- Dresback KM, Blain CA, Kolar RL (2004) Resolution and algorithmic influences on the baroclinic pressure gradient in finite element based hydrodynamic models. In: C. T. Miller, et al. (eds) Computational Methods, Surface Water Systems and Hydrology, vol. 2. pp 1755–1766
- Dresback K, Kolar RL, Blain CA, Cambazoglu MK, Shay T, Luettich RA (2010) Development and application of the coupled HYCOM and ADCIRC system. In: Spaulding ML (ed) Estuarine and coastal modeling, proceedings of the 11th international conference. American Society of Civil Engineers, Seattle, pp 259–277
- Egbert G, Erofeeva S (2002) Efficient inverse modeling of barotropic ocean tides. *J Atmos Ocean Technol* 19:183–204
- Egbert GD, Bennett AF, Foreman MGG (1994) TOPEX/POSEIDON tides estimated using a global inverse model. *J Geophys Res* 99:24821–24852
- Garratt JR (1977) Review of drag coefficients over oceans and continents. *Mon Weather Rev* 105:915–929
- Hallock ZR, Pistek P, Book JW, Miller JL (2003) A description of tides near the Chesapeake Bay entrance using in situ data with an adjoint model. *J Geophys Res* 108:3075–3083
- Hannah C, Wright DG (1995) Quantitative skill assessment for coastal ocean models. Coastal estuarine studies. Depth dependent analytical and numerical solutions for wind-driven flow in the coastal ocean, vol 47. American Geophysical Union, Washington, DC, pp 125–152
- Hench JL, Luettich RA (2003) Transient tidal circulation and momentum balances at a shallow inlet. *J Phys Oceanogr* 33:913–932
- Hodur RM (1997) The naval research laboratory’s coupled ocean/atmosphere mesoscale prediction system (COAMPS). *Mon Weather Rev* 135:1414–1430
- Johnson DR (1995) Wind forced surface currents at the entrance to Chesapeake Bay: their effect on blue crab larval dispersion and post-larval recruitment. *Bull Mar Sci* 57:726–738
- Kara AB, Barron C, Martin P, Smedstad L, Rhodes R (2006) Validation of interannual simulations from the 1/8 global Navy Coastal Ocean Model (NCOM). *Ocean Model* 11(3–4):376–398. doi:10.1016/j.ocemod.2005.01.003
- Ko DS, Martin PJ, Rowley CD, Preller RH (2008) A real-time coastal ocean prediction experiment for MREA04. *J Mar Syst* 69(1–2):17–28
- Kolar RL, Kibbey TCG, Szpilka CM, Dresback KM, Tromble EM, Toohey IP, Hoggan JL, Atkinson JH (2009) Process-oriented tests for validation of baroclinic shallow water models: the lock-exchange problem. *Ocean Model* 28(1–3):137–152
- Kurapov AL, Egbert GD, Miller RN, Allen JS (2002) Data assimilation in a Baroclinic coastal ocean model: ensemble statistics and comparison of methods. *Mon Weather Rev* 130:1009–1025
- Li M, Zhong L, Boicourt WC (2005) Simulations of Chesapeake Bay estuary: sensitivity to turbulence mixing parameterizations and comparison with observations. *J Geophys Res* 110:12004–12026
- Li Z, Chao Y, McWilliams JC, Ide K (2008) A three-dimensional variational data assimilation scheme for the regional ocean

- modeling system: implementation and basic experiments. *J Geophys Res* 113. doi:[10.1029/2006JC004042](https://doi.org/10.1029/2006JC004042)
- Logotov OG (2008) A multigrid methodology for assimilation of measurements into regional tidal models. *Ocean Dyn* 58:441–460
- Logotov OG, Lermusiaux PFJ (2008) Inverse barotropic tidal estimation for regional ocean applications. *Ocean Model* 25:17–34
- Luettich Jr R, Westerink JJ (2004) Formulation and numerical implementation of the 2D/3D ADCIRC finite element model version 44.XX. <http://www.adcirc.org>
- Luettich RA, Muccino JC, Foreman MGG (2002) Considerations in the calculation of vertical velocity in three-dimensional circulation models. *J Atmos Ocean Technol* 19:2063–2076
- Lyard F, Lefevre F, Letellier T, Francis O (2006) Modelling the global ocean tides: modern insights from FES2004. *Ocean Dyn* 56(5–6). doi:[10.1007/s10236-006-0086-x](https://doi.org/10.1007/s10236-006-0086-x)
- McDougall TJ, Wright DG, Jacket DR, Fiestel R (2003) Accurate and computationally efficient algorithms for temperature and density of seawater. *J Atmos Ocean Technol* 20(5):730–741
- Mellor GL (1996) Introduction to physical oceanography. Springer, Princeton
- Mellor GL, Yamada T (1982) Development of a turbulence closure model for geophysical fluid problems. *Rev Geophys Space Phys* 20:851–875
- Muccino JC, Gray WG, Foreman MGG (1997) Calculation of vertical velocity in three dimensional shallow water equation, finite element models. *Int J Numer Methods Fluids* 25(7):779–802
- Mukai A, Westerink J, Luettich R, Mark D (2002) A tidal constituent database for the Western North Atlantic Ocean, Gulf of Mexico and Caribbean Sea. Tech. rep. ERDC/CHL TR-02-2. US Army Engineer Research and Development Center, Vicksburg
- National Center for Environmental Prediction (NCEP) (2010) ocean prediction center. http://www.opc.ncep.noaa.gov/newNCOM/NCOM_currents.shtml
- NOAA National Ocean Service (NOS) (2011) Tidal harmonics for Chesapeake Bay Bridge Tunnel, VA, station ID: 8638863. Tides and currents WWW page. <http://tidesandcurrents.noaa.gov/oaatidepredictions/NOAATidesFacade.jsp?Stationid=8638863>
- Rosmond TE, Teixeira J, Peng M, Hogan TF, Pauley R (2002) Navy Operational Global Atmospheric Prediction System (NOGAPS): forcing for ocean models. *Oceanography* 15(1):99–108
- Shay LK, Cook TM, Hallock ZR, Haus B, Graber HC, Martinez J (2001) The strength of the M_2 tide at the Chesapeake Bay mouth. *J Phys Oceanogr* 31:427–449
- Shchepetkin AF, McWilliams J (2005) The regional ocean modeling system: a split-explicit, free-surface, topography-following coordinates ocean model. *Ocean Model* 9:347–404
- Westerink J, Luettich R, Feyen J, Atkinson J, Dawson C, Roberts H, Powell M, Dunion J, Kubatko E, Pourtaheri H (2008) A basin to channel scale unstructured grid hurricane storm surge model applied to Southern Louisiana. *Mon Weather Rev* 136:833–864
- Wilmott CJ (1981) On the validation of models. *Phys Geogr* 2:184–194
- Yang Z, Myers E, White S (2007) The Chesapeake and Delaware Bays VDatum development and progress towards a national VDatum. http://www.thsoa.org/hy07/04P_13.pdf